ARL 66-0111
JUNE, 1966

Aerospace Research Laboratories

VISCOUS HYPERSONIC FLOWS OVER POINTED CONES AT LOW REYNOLDS NUMBERS

H. F. WALDRON

CORNELL AERONAUTICAL LABORATORY, INC.
BUFFALO, NEW YORK

CONTRACT AF 33 (615)-1205
PROJECT 7064

OFFICE OF AEROSPACE RESEARCH
United States Air Force

ARL 66-0111

VICOUS HYPERSONIC FLOWS OVER POINTED CONES AT LOW REYNOLDS NUMBERS

H. F. WALDRON

CORNELL AERONAUTICAL LABORATORY, INC.
BUFFALO, NEW YORK

JUNE, 1966

CONTRACT AF 33 (615)-1205
PROJECT 7064

AEROSPACE RESEARCH LABORATORIES
OFFICE OF AEROSPACE RESEARCH
UNITED STATES AIR FORCE
WRIGHT-PATTERSON AIR FORCE BASE, OHIO

FOREWORD

This interim technical report was prepared by the Aerodynamic Research Department of Cornell Aeronautical Laboratory, Inc., Buffalo, New York on Contract AF 33(615)-1205 for the Aerospace Research Laboratories, Office of Aerospace Research, United States Air Force. The research reported herein was accomplished on Project 7064, "High Velocity Fluid Mechanics," under the technical cognizance of Mr. Anthony W. Fiore of the Hypersonic Research Laboratory of ARL.

The author wishes to acknowledge the contribution of Mr. C. E. Wittliff, who assisted in the preparation of this report.

ABSTRACT

An experimental and analytical study of viscous hypersonic flow over pointed cones with particular emphasis on the viscous-layer regime is presented. Shock tunnel measurements of heat transfer to 5°, 10° and 20° half-angle cones and of pressure on the 20° cone are compared with the predictions of a viscous-inviscid interaction analysis (Probstein and Elliot) including transverse curvature, of a viscous-layer nonslender cone analysis (Cheng) and of an extension of the nonslender cone analysis incorporating effects of slenderness. The large rise in heat transfer predicted by the transverse curvature theory is not observed and close agreement is obtained with the nonslender cone viscous-layer predictions. An extension of the nonslender cone analysis is presented where the effects of cone slenderness are included by a perturbation analysis. The solution of the resulting equations reveals that the net effect of transverse curvature and of other effects associated with cone slenderness is small in the viscous-layer regime for not-too-slender cones. Good agreement of the 10° and the 20° cone experimental data is obtained with this extension of the nonslender solution.

TABLE OF CONTENTS

NOTATION

A, B	integration constants determined from the shock and wall boundary conditions, respectively
a_N	coefficients of a series expansion defined by Equation (14a)
c	constant of proportionality between temperature and viscosity
C_H	Stanton number defined as $C_H \equiv \frac{c_p}{Pr}\left(\mu \frac{\partial T}{\partial y}\right)_{y=0} \Big/ \rho_\infty u_\infty (H_\infty - H_w)$
H	total enthalpy
k_1	defined by $\mu_w = k_1 \lambda_w \rho_w \sqrt{\gamma R T_w}$
K^2	rarefaction parameter for a blunt axisymmetric body defined as $K^2 \equiv \frac{\epsilon \rho_\infty u_\infty a}{\mu_0}\left(\frac{\mu_0}{\mu_*}\frac{T_*}{T_0}\right)$ where a is nose radius
M	Mach number
Pr	Prandtl number
$p, \bar{p}$	pressure $\bar{p} = p/\rho_\infty U_\infty^2 \sin^2\beta$
q	heat transfer rate
$Q(\bar{x}, \zeta)$	defined by Equation A-10 (a)
r_0	cone radius = $x \sin\theta_c$
r	$r_0 + y \cos\theta_c$
R	radius of curvature of streamlines
Re_x	Reynolds number
T	temperature
T_0	stagnation temperature
T_*	reference temperature used in the determination of the constant of proportionality in the linear representation $\mu = C_* \frac{\mu_*}{T_*} T$
u_∞	free stream velocity
u, v	velocity components in the x, y direction
$\bar{u}_0$	zero order solution for velocity, $\bar{u}_0 = \alpha_0 \zeta$

$\bar{u}$ $u/u_\infty \cos\beta$

$\bar{v}$ $v/\epsilon u_\infty \sin\beta$

W $\bar{u}^2/2$

x, y coordinates parallel and perpendicular to cone surface

$\bar{\varkappa}$ cone and wedge rarefaction parameter

$$\bar{\varkappa} \equiv \frac{\epsilon \rho_\infty u_\infty x \sec\beta}{\mu_0}\left(\frac{\mu_0}{\mu_*}\frac{T_*}{T_0}\right) = \frac{Re_{x_\infty}}{\gamma M_\infty^2 C_* \cos\theta_c}$$

α_0 power series in $\bar{x}$ where $\bar{u} = \alpha_0 \zeta$ defined by Equation (4)

β shock angle

γ ratio of specific heats

δ boundary layer thickness

ϵ $(\gamma-1)/2\gamma$

ζ nondimensional form of the stream function defined by

$$\zeta^2 \equiv \psi/\rho_\infty u_\infty \pi r^2$$

Θ $(H-H_w)/(H_\infty - H_w)$

θ_c cone half-angle

$\lambda_w, \lambda_j, \lambda_s - \lambda_w$ mean free path at the wall, $\lambda_j \simeq \frac{2\gamma}{\gamma+1}\lambda_w$, $\lambda_s \simeq \lambda_w$ for unit accommodation coefficients

$\bar{\lambda}$ $\frac{\lambda_s}{\lambda_w}\frac{1}{k_1 \bar{x}\sin\beta}\sqrt{\epsilon\frac{T_w}{T_0}}$

μ viscosity

ρ density

φ $2\pi r \rho_\infty u_\infty \zeta^2 \left(\frac{\partial r}{\partial \psi}\right)_x$

$\bar{\tau}$ $M^3\sqrt{C/Re_x}$

ψ stream function, $\frac{\partial \psi}{\partial y} = 2\pi r \rho u \qquad \frac{\partial \psi}{\partial x} = -2\pi r \rho v$

Subscripts

$w, \infty, 0$ pertaining to wall, free stream and stagnation conditions

M pertaining to solution of flow field using Mangler's transformation

c pertaining to inviscid cone flow

s conditions behind shock except Surface Slip Effects in the Appendix where it refers to solution including surface slip effects

$*$ based on reference temperature T_*

1. INTRODUCTION

The departures from the classical thin boundary layer concept due to a high degree of flow rarefaction at high Mach numbers are of considerable current interest. The relative importance of the phenomena causing such departures is closely allied to many factors such as the surface to stagnation temperature ratios, the geometry of the body which is generating the boundary layer and the ambient conditions. Among the basic body geometries, such as the sphere, the flat plate, the wedge, and the cone, viscous hypersonic flows over cones at low Reynolds numbers have received the least attention. The present paper reports an investigation of flow over pointed cones with emphasis on heat transfer in a flow regime where the shock layer is fully viscous; that is, where the concept of both an inviscid and a viscid layer is no longer valid. In particular, this study investigates the regime of applicability of the theoretical model of the viscous-layer regime postulated by Cheng.[1] The model utilizes the Navier-Stokes equations and the thin shock-layer concept where the Rankine-Hugoniot relations are modified to account for the effects of transport processes at the shock.

This viscous-layer model has been applied to the blunt axisymmetric body, the wedge, and the nonslender cone.[1] Experimental measurements of heat transfer[2,3] have confirmed the validity of this flow model (as far as the prediction of heat transfer is concerned) except for the case of the cone which is the subject of the current study. The recent work of Vidal and Bartz[2] in which heat transfer and pressure distributions have been obtained on a wedge shows good agreement with the theoretical predictions for wedge angles between 20° and that required for shock wave detachment. They conclude that the lack of correlation for smaller wedge angles is largely due to the neglect

Manuscript released by the author January 1966 for publication as an ARL Technical Report.

of the viscous-layer thickness in comparison with the wedge thickness. Their measurements span the transition from continuum to near-free-molecule flow.

The flow field over a pointed cone encompasses many of the flow regimes of fluid mechanics from the classical thin boundary-layer and inviscid outer flow at large distances downstream to free molecule flow at the cone vertex. As the Reynolds number decreases below that where the thin boundary-layer analysis applies, the ratio of boundary-layer thickness to body radius (δ/r_s) increases and the influence of the boundary-layer growth on the flow must be considered. The majority of the theoretical and experimental investigations for viscous flow about pointed cones (for example, References 4-7) have dealt with the effects of the interaction of viscid and inviscid layers and of transverse curvature (circumferential spreading of the boundary layer) under the condition that $\delta/r_s < 1$. As the Reynolds number further decreases separate viscid and inviscid layers no longer exist and the shock layer is fully viscous, even for a ratio of shock-layer thickness to body radius less than unity. In this regime the only available theoretical model[1] (to the author's knowledge) relies on the thin shock-layer approximations and is thus restricted to nonslender bodies. Also, in this regime, there appear to be no previous experimental data for either slender or nonslender cones.

The main purpose of the present study was to investigate experimentally the range of applicability of Cheng's nonslender-cone viscous-layer[1] analysis and to examine the relative effect of the parameters associated with slenderness on heat transfer and other flow-field properties. Shock tunnel measurements of heat transfer to 5°, 10°, and 20° half-angle cones and of surface pressure on a 20° cone have been obtained. These measurements cover a range of Mach numbers from 19 to 24, Reynolds number per inch from 150 to 4000 and are for a wall to stagnation temperature ratio of about 0.08. A comparison of the experimental data with the predictions of the nonslender-cone analysis

shows surprisingly good agreement even for the 5° cone. This agreement implies that the slenderness effect on heat transfer and pressure due to increasing cone slenderness is small in the viscous-layer regime.

In addition to the experimental study, a perturbation analysis is presented to incorporate the role of slenderness on heat transfer in the viscous-layer regime. This solution which uses an analytical form of the nonslender-cone solution includes the effects of shock transport, viscous-layer displacement, shock curvature, transverse curvature and surface slip* as higher-order terms.

In Section 2 of this paper, a brief review of the existing theories of viscous flows over pointed cones is presented including the viscous-inviscid interaction and the viscous-layer regimes. Although the primary interest of the present investigation is in the regime where the shock layer is fully viscous, some of the viscous-inviscid interaction theories are discussed. These latter theories represent the only previous theoretical investigations of the effects of cone slenderness on heat transfer and as such represent a high Reynolds number limit of the heat transfer. The experimental apparatus and techniques are next discussed in Sec. 3. Then in Sec. 4, a comparison is presented of the experimental data with viscous-inviscid interaction predictions, with the nonslender-cone viscous-layer predictions and with the perturbation solution incorporating the effects of slenderness. Although the results of this perturbation solution are presented and discussed in Section 4, the details of the solution are given in the Appendix.

2.0 REVIEW OF THEORETICAL STUDIES

2.1 Viscous-Inviscid Interaction Regime Including Transverse Curvature

In the weak-interaction regime the now classical papers are those by Probstein[4] and Probstein and Elliot.[5] By reducing the boundary-layer

*Surface slip effects will be used in this paper to encompass both slip and temperature jump effects.

equations to an almost two-dimensional form through a modified Mangler transformation the effects of viscous-inviscid interaction[4] and transverse curvature[5] have been separately studied for $\delta/r_0 < 1$. Their results show that boundary-layer displacement has a negligible effect on heat transfer, but does affect wall pressure. On the other hand, the transverse curvature affects only the heat transfer. For $Pr = 1$, the heat transfer[5] is given in terms of the external flow properties as

$$\left(\frac{q}{q_M} - 1\right) = \frac{\gamma(\epsilon/Re_x)_c}{\sqrt{3}\tan\theta_c}\left[0.517 + 0.913\,\frac{T_w}{T_c} + 0.12\,(\gamma-1)M_c^2\right] \qquad (1)$$

The value of q_M, the heat transfer in the classical boundary-layer regime, is given by the solution to the boundary-layer equations utilizing the Mangler transformation as $q_M = \rho_c u_c (H_e - H_w)(0.332\sqrt{3})\sqrt{(\epsilon/Re_x)_c}$

The pressure[4] is given by

$$\left(\frac{p}{p_c} - 1\right) = F_1(K)\,\alpha_\infty\,\bar{\tau}_c + F_2(K)\,\alpha_\infty^2\,\bar{\tau}_c^2 \qquad (2)$$

where $F_1(K)$ and $F_2(K)$ are functions of the hypersonic similarity parameter given in Reference 4 and

$$\alpha_\infty = \frac{0.968}{M_\infty^2}\,\frac{T_w}{T_\infty} + 0.145 \qquad \text{for} \quad Pr = 1$$

The effect of transverse curvature on the boundary-layer growth, considered of higher order by Probstein,[4] has been studied by Yasuhara[8] for $\delta/r_0 \leq 1$. He obtains a self-similar solution corresponding to a strong shock interacting with the boundary layer. This solution is applicable to a slender power-law body which grows as $x^{3/4}$. A solution is also obtained for a slender cone using the local similarity method from which the boundary-layer growth is expressed in terms of a curvature parameter $\bar{\tau}_c / M_c\theta_c$. The results of this study show that the displacement thickness is overestimated as a result of neglecting transverse curvature on boundary-layer growth. By

using Van Dyke's supersonic-hypersonic similarity rule, Yasuhara shows that neglect of the transverse curvature term also overestimates the surface pressure. Recently, Stewartson[9] has obtained a solution for the strong-interaction regime over slender cones; where the changes in the outer inviscid cone due to increasing boundary-layer thickness are permitted to influence the boundary-layer growth.

For the present range of experimental variables, the predictions of both Yasuhara's and Stewartson's analyses are not significantly different from those of Probstein. Thus, the relationships given by Equations (1) and (2) adequately represent the effect of cone slenderness on heat transfer and surface pressure in the viscous-inviscid interaction regime and as such are utilized for comparison with the experimental data and for comparison with the predictions of the viscous-layer analysis.

2.2 Viscous-Layer Regime

The only solution for flows over pointed cones where the shock layer is fully viscous (Cheng, Reference 1) is formulated from the Navier-Stokes equations and is based on thin shock-layer approximations. In this solution, the effects of surface slip, viscous-layer displacement, transverse curvature and shock curvature are considered unimportant compared to the slip-like velocity and enthalpy changes across the shock. The solution is applicable to highly cooled surfaces and nonslender cones where $\delta/r_o \ll 1$. Under the assumptions of a thin shock-layer, a perfect gas with constant specific heats, a linear viscosity-temperature law and unit Prandtl number, the solution to the flow field is reduced to the solution of a single parabolic differential equation governing the velocity. This equation in terms of a nondimensionalized velocity u_o and a stream function (ζ) is given by

$$\bar{x}\,\bar{u}_o \frac{\partial \bar{u}_o}{\partial \bar{x}} = \zeta\,\bar{u}_o \frac{\partial \bar{u}_o}{\partial \zeta} + \frac{u_o}{\zeta \bar{x}} \frac{\partial}{\partial \zeta}\left(\frac{\bar{u}_o}{\zeta} \frac{\partial \bar{u}_o}{\partial \zeta}\right) \qquad (3a)$$

with the shock boundary condition at $\zeta = 1$

as
$$\bar{u}_0(1) = 1 - \left(\frac{\bar{u}_0}{\bar{x}}\frac{\partial \bar{u}_0}{\partial \zeta}\right)_{\zeta=1} \tag{3b}$$

A numerical solution to Equations (3) has been obtained by Cheng[1] using an implicit finite-difference scheme. The starting value for the forward integration was obtained by a series expansion solution in $\bar{x}$ in a form which satisfies the differential equation, the shock boundary condition and no slip at the surface. The numerical solution reveals that the velocity profile closely follows the Blasius profile down to a value of $\bar{x} \simeq 3$ even though the shock layer is fully viscous at this value. At values of $\bar{x} < 1$ the velocity profile is linear in ζ and can be adequately represented by the first four terms of the series expansion solution in the form

$$\bar{u}_0 = \alpha_0 \zeta \tag{4}$$

where

$$\alpha_0 = \bar{x}^{1/2} - \frac{5}{12}\bar{x} + \frac{187}{12^2 \cdot 20}\bar{x}^{3/2} - \frac{3085}{12^3 \cdot 100}\bar{x}^2$$

The surface heat transfer, as computed from the series expansion solution, converges to the free-molecule limit for unit accommodation coefficient and to the boundary-layer limit at high Reynolds numbers. In Reference 1, a divergence is shown between the heat transfer predicted by the series expansion solution and that by the numerical solution in the vicinity of $\bar{x} \simeq 1$. However, by writing $C_H/\sin\beta = \frac{1}{\bar{x}}\left(\frac{\bar{u}_0}{\zeta}\frac{\partial \bar{u}_0}{\partial \zeta}\right)_{\zeta=0}$ and substituting the linear form of $\bar{u}_0$, the value of heat transfer is

$$\frac{C_H}{\sin\beta} \simeq \frac{\alpha_0^2}{\bar{x}}$$

which follows the numerical solution for $\bar{x} > 1$ and converges to the classical boundary-layer solution. Cheng's solution assumes the pressure in the viscous layer as constant and equal to the Newtonian value based on the shock angle (i.e., $p/p_\infty = \gamma M_\infty^2 \sin^2\beta$).

The solution for the flow field about a nonslender cone predicts the flow field in terms of a single parameter $\bar{\varkappa}$ in which all effects of surface incidence and rarefaction are included. In the analysis presented in the Appendix, a solution for the flow field based on a perturbation analysis is obtained where the zero-order solution is the solution for the nonslender cone. This analysis incorporates some of the higher-order terms neglected by Cheng; that is, transverse curvature, viscous-layer displacement, shock curvature, shock angle different from body angle and surface slip effects.

3. EXPERIMENTAL APPARATUS AND TECHNIQUES

3.1 The Six-Foot Shock Tunnel

The experimental data presented in this paper were obtained in the CAL Six-Foot Shock Tunnel. This conventional shock tunnel operating on the tailored-interface principle is capable of producing hypersonic flows over a wide range of Mach and Reynolds numbers. Since a complete description of this facility and the full range of operating conditions are given by Hilton et al,[10] only the details which have a bearing on the present investigation will be given here.

The tunnel was operated with air at a reservoir temperature of about 4000°K and reservoir pressures from 12 to 300 atm. The reservoir conditions were generated by a shock at a Mach number of about 6 with a 70% H_2 + 30% He driver gas heated to about 675°K. The test-section Mach number was varied by operating at two different nozzle area ratios* as well as by the changes in the nozzle boundary-layer thickness resulting from the Reynolds number variations. The resultant test-section flow covers a range of free-stream

*The tunnel is equipped with a two-stage nozzle. A rectangular throat of height 0.200" was used for the present experiments. The inlets to the second stage conical nozzle were 1-1/2" and 2-5/8" in diameter.

Mach number from 19 to 24 and of Reynolds number per inch from 150 to 4000 (when the effects of thermochemical nonequilibrium nozzle expansion are included as discussed subsequently).

The second-stage nozzle is canted at an angle of 10° to the shock tube centerline to eliminate the diaphragm particles in the test section and hence permits flow studies over relatively delicate models. The tunnel nozzle is separated from the shock tube by a diaphragm and the pressure in the tunnel was less than 0.1 micron Hg prior to firing mainly to minimize starting times.

3.2 Test-Section Flow and Calibration

The test-section flow properties are determined by calculating the thermochemical nonequilibrium expansion from the reservoir conditions to the measured test-section pitot pressure. The reservoir conditions are determined from the measured incident shock speed, equilibrium air calculations, and the measured reservoir pressure. Departures from ideal tailored-interface conditions are taken into account by assuming that isentropic wave processes caused the observed departures. The equilibrium test-section conditions are determined under the assumption of an isentropic expansion from the measured reservoir pressure, the hypersonic approximation $H_o \simeq \frac{1}{2} u_\infty^2$ and $p_o' \simeq \rho_\infty u_\infty^2 \left[1 - \frac{1}{2}\frac{\rho_\infty}{\rho_s}\right]$ where ρ_∞/ρ_s is the density ratio across a normal shock wave. The calculated equilibrium test-section conditions are then corrected to account for the nonequilibrium nozzle expansion. These correction factors are determined from a computer program previously developed at CAL[11] by computing both equilibrium and nonequilibrium nozzle expansion to the measured value of pitot pressure (vibration is assumed in equilibrium but air chemistry is not). This technique has been described by Vidal and Wittliff[3] who tabulated correction factors. The accompanying Table I gives these factors for the present operating conditions. The

thermochemical nonequilibrium effects are most significant at the lowest reservoir pressure involving a factor of about 1.8 for the ratio of the non-equilibrium-to-equilibrium values of Reynolds numbers.

Table I

NOZZLE NONEQUILIBRIUM EFFECTS ON THE AERODYNAMIC PARAMETERS

T_o = 4000°K

p_R	12 atm	25 atm	100 atm	300 atm
$(C_H)_N / (C_N)_E$	1.098	1.068	1.037	1.013
$(M_\infty)_N / (M_\infty)_E$	1.175	1.123	1.044	1.023
$(Re)_N / (Re)_E$	1.800	1.543	1.220	1.090
$\left(M\sqrt{C_H/Re}\right)_N / \left(M\sqrt{C_H/Re}\right)_E$	0.8757	0.9363	0.9643	0.9881
$(p/p_\infty)_N / (p/p_\infty)_E$	1.350	1.260	1.090	1.046
$(\bar{x})_N / (\bar{x})_E$	1.305	1.135	1.065	1.025

In view of the rather significant departures of the test-section flow properties from the equilibrium nozzle expansion, measurement of flow Mach number was obtained independent of pitot pressure and reservoir conditions. A free-molecule probe* was used which measures heat transfer of two parallel flat plates and to the stagnation point of a cylinder. Utilizing two-dimensional free-molecule flow theory and the assumption that the accommodation coefficients for the flat plate and cylinder are equal, the ratio of stagnation-point heat transfer to flat-plate heat transfer is directly proportional to the free stream Mach number (for large Mach number).

---

*The author is indebted to R.J. Vidal and J.A. Bartz of the Aerodynamic Research Department of Cornell Aeronautical Laboratory for the use of the free-molecule probe which was developed for other studies of low density flows under Contract AF 49(638)-1433.

$$M_\infty = \sqrt{2\pi\gamma}\ \frac{\text{Stagnation point heat transfer}}{\text{Flat plate heat transfer}}$$

For Knudsen numbers > 10, the Mach number as determined from the probe agreed to within 10% with the Mach number as determined from the pitot pressure, reservoir conditions and nozzle nonequilibrium corrections. For Knudsen numbers less than 10, the use of the free-molecule probe for determination of Mach number is not justified.

The flow angularity was also determined from the free-molecule probe. Since the thin-film gauges are located on opposite sides of the two flat plates, the flow is parallel to the probe axis when the heat transfer rates to the two plates are equal. By measuring the heat transfer to the two flat plates at various angles, flow angularity may be determined to within ±0.1°. The flow in the uniform core (as determined from pitot pressure measurements) was found to be parallel to the tunnel centerline to within ±0.1°.

3.3 Models and Instrumentation

The experimental measurements were obtained on the three pointed cones with half-angles of 5°, 10°, and 20° shown in Figure 1. Heat transfer data were obtained by means of platinum thin-film resistance thermometers[12] on all models and pressure distributions from piezoelectric pressure transducers on the 20° cone.

The measured surface temperatures are converted to heat transfer rates by analogue circuits.[13] Since heat transfer rates less than 1 Btu/ft^2/sec. were measured, special low-noise amplifiers were employed. Heat transfer and pressure data were recorded on rotating drum oscilloscopes with sweep speed of 200μsecs/cm. The cone models were sting mounted on the shock tunnel centerline. However, in some tests, both the 10° and 20° cones were mounted side by side to provide simultaneous recording of data from both models.

The 5° cone was constructed of Pyrex glass with a brass tip. The first of six thin-film gauges painted on the surface is located approximately 1" from the cone vertex. A thin layer of gold painted on the cone surface acts as the electrical connection from the platinum elements to the base of the model where the wires leading to the amplifiers and recording devices are soldered. The resistance of the leads is made approximately 1/10 the resistance of the elements in order to reduce the effect on the data of resistance changes in the leads. The platinum elements are electrically insulated by a thin layer of titanium dioxide, whereas the leads and connections are insulated with a relatively thicker layer of glyptol paint. The glyptol coating on the leads further reduces any effect of changes in lead resistance on measured data since the glyptol is a good thermal insulator compared to the titanium dioxide.

The 10° cone is constructed entirely of Pyrex glass with a nose radius of approximately 0.005". This model has four platinum elements on the cone surface constructed in an identical manner as those on the 5° cone. The first heat transfer gauge is located at a distance of 0.075" from the cone vertex. Although this first gauge has a very thin Pyrex backing due to the small cone diameter at this location, heat conduction into the Pyrex is negligible during the test period. The cone tip showed no evidence of ablation at the completion of the tests, indicating both small temperature rise due to the air flow and an absence of diaphragm particles or other tunnel debris impinging on the cones.

The 20° cone is fabricated entirely from brass with recesses on the surface to incorporate pressure transducers and small Pyrex buttons on which the platinum elements are painted. The leads are internal to the cone body. Each pressure transducer is located at the bottom of an orifice of 0.125" diameter and 0.100" depth. The high degree of flow rarefaction necessitated a correction to the measured pressure to account for orifice and thermal

transpiration effects. An empirical formula obtained by Knudsen was used to correct the pressure data. Although not strictly applicable to the present orifice geometry and flow field, this formula and its experimental verification for similar flows are discussed by Vidal and Bartz.[2] They compared the corrected pressures to pressures measured with flush mounted transducers for wedges and flat plates under conditions where the correction reached 50% of the measured orifice value. Since an empirical verification has been obtained[2] for comparable flows, the present pressure data have been corrected in the manner discussed by Vidal and Bartz.

4. RESULTS AND DISCUSSION

In this section, the experimental data are compared with the prediction of Probstein's viscous-inviscid interaction analysis,[4] of Probstein and Elliot's transverse curvature theory[5] and with Cheng's nonslender-cone viscous-layer analysis.[1] In order to reveal the role of transverse curvature and other effects associated with slenderness and to provide a better correlation of the experimental data, an analysis is developed in the Appendix to account for some of the effects of slenderness in the viscous-layer regime. The predictions of this analysis incorporating slenderness are also compared with the experimental heat transfer and pressure data.

4.1 The Viscous-Inviscid Interaction Regime Including Transverse Curvature

The prediction for heat transfer due to the first-order effect of transverse curvature is given by Equation (1). The prediction of pressure due to the interaction of the viscous and inviscid layers is given by Equation (2). These equations express heat transfer in terms of the classical boundary-layer value and pressure in terms of the local inviscid value as functions of the local inviscid-flow parameters. Although the theoretical predictions of heat transfer

and pressure can be expressed in terms of the free-stream conditions by utilizing tangent-cone predictions[14] for the inviscid flow field, this does not reveal a free-stream parameter. However, by utilizing the Newtonian pressure value $p/p_\infty = \gamma M_\infty^2 \sin^2\theta_c$, $u_c \simeq u_\infty$, a strong shock approximation for density and letting $\sin\theta_c \simeq \tan\theta_c$ it can be shown that

$$\frac{C_H}{\sin^3\theta_c} = f_1\left[\frac{M_\infty}{\sin^2\theta_c}\sqrt{\frac{C_*}{Re_{x_\infty}}}\,,\ \sin^2\theta_c\right] \tag{5}$$

and

$$\frac{p/p_\infty}{\gamma M_\infty^2 \sin^2\theta_c} = f_2\left[\frac{M_\infty}{\sin^2\theta_c}\sqrt{\frac{C_*}{Re_{x_\infty}}}\right]$$

where C_*, the constant of proportionality between temperature and viscosity, is based on a reference temperature T_* given by (for cone flows)

$$\frac{T_*}{T_w} = \frac{T_w}{T_o} + \frac{1}{2}\left(1 - \frac{T_w}{T_o}\right) - \frac{1}{3}\cos^2\theta_c \tag{6}$$

Although the assumption of a linear viscosity-temperature relation may lead to certain discrepancies, it has been shown[15] that the selection of such a reference temperature significantly reduces these discrepancies.

The variables in the expression for heat transfer and pressure determined from Equations (1) and (2) are consistent with hypersonic viscous similitude. The question of similitude has been examined by Cheng[16] for pointed cones including the boundary-layer displacement effect but not transverse curvature. For the case involving strong shock waves, unit Prandtl number, linear viscosity-temperature relation, he has shown that $C_H/\sin^3\theta_c$ and $(p/p_\infty)/\gamma M_\infty^2 \sin^2\theta_c$ can be expressed as functions of the free-stream parameter $\frac{M_\infty}{\sin^2\theta_c}\sqrt{\frac{C_*}{Re_{x_\infty}}}$. Actually, he gives the parameter

$$\left(\frac{\gamma-1}{\gamma+1}\right)\left[0.664+1.73\,\frac{T_w}{T_o}\right]\frac{M_\infty}{\sin^2\theta_c}\sqrt{\frac{C_*}{Re_{x_\infty}}}$$

However, since T_w/T_o is constant in the present experiments, that term can be omitted. The functional dependence for $C_H/\sin^3\theta_c$ (Equation (5) developed from Probstein and Elliot's analysis[5] includes an additional parameter $\sin^2\theta_c$ due to transverse curvature.

The heat transfer and pressure data are compared with the predictions of the interaction analysis in Figures 2 and 3. For convenience, the heat transfer dependence has been transposed to the form

$$\frac{M_\infty^2}{\bar{\iota}_\infty}\frac{C_H}{\sin^2\theta_c}=f_3\left[\frac{M_\infty}{\sin^2\theta_c}\sqrt{\frac{C_*}{Re_{x_\infty}}}\,,\ \sin^2\theta_c\right]$$

The slight dependence of pressure on the cone angle in Figure 3 results from the utilization of the tangent-cone predictions[14] for the inviscid flow field. The free-molecule limit shown in Figures 2 and 3 has been computed from the formulae given on pages 401-403 of Reference 14. For large free-stream Mach numbers and $M_\infty \sin\theta_c > 1$ (valid for the current experiments) the free-molecule limit for heat transfer is adequately given by $\sin\theta_c$, the value for infinite speed ratio and completely diffuse reflection. The free-molecule limit for pressure for completely diffuse reflection is given by

$$\frac{(p/p_\infty)}{\gamma M_\infty^2\sin^2\theta_c}=1+\frac{\sqrt{\frac{\pi(\gamma-1)}{4\gamma}}}{\sin\theta_c}\sqrt{\frac{T_w}{T_o}}$$

when $\sqrt{\frac{\gamma}{2}}\,M_\infty \sin\theta_c \gg 1$. Additional shock-tunnel data[17] obtained at higher Reynolds numbers than the present data are also included in Figures 2 and 3. These data were obtained by Wilkinson and Harrington in the CAL 48" hypersonic shock tunnel. Bearing in mind that there is a slight difference in cone angles, the two sets of data appear consistent. The heat transfer data in

Figure 2 depart from the predictions of the interaction analysis at about $\frac{M_\infty}{\sin^2\theta_c}\sqrt{\frac{C_H}{Re_{x_\infty}}} \simeq 3$. At values of this parameter greater than about 20, (for the 5° and 10° cones) it is seen that $\frac{M_\infty^2}{\bar{\chi}_\infty}\frac{C_H}{\sin\theta_c}\left(1-\frac{T_w}{T_o}\right)$ is dependent on cone angle. The data appear to be converging to the free-molecule limit even though the largest Knudsen number is only about 2-1/2 for the 10° cone (Knudsen number is taken as the ratio of mean-free-path to the distance of the first heat transfer gauge from the cone vertex).

The pressure data in Figure 3 exhibit a somewhat similar effect to the heat transfer except that the departures are smaller. The data for the small cone angles from Reference 17 follow the prediction of the interaction analysis reasonably well, whereas, the present data for the 20° cone fall slightly below the prediction.

4.2 The Viscous-Layer Regime for Nonslender Cones

In the viscous-layer regime, the heat transfer to nonslender cones expressed as $C_H/\sin\beta$ is a function of the single parameter $\bar{\chi}$. A comparison of the theoretical prediction and the experimental data is shown in Figure 4. In this figure, the experimental values of Stanton number C_H are divided by the cone half-angle rather than the shock angle. It is seen that surprisingly good correlation is obtained over almost the entire range of $\bar{\chi}$ and that the dependence of $C_H/\sin\theta_c$ on cone angle is small.

Although the dependence of $C_H/\sin\theta_c$ on cone angle is small, a definite difference exists among the 5° and 6.3° cones, the 9° and 10° cones, and the 20° cone. The heat transfer data presented for the 6.3° cone[17] depart from the transverse-curvature prediction at about $\bar{\chi} = 100$ and as $\bar{\chi}$ decreases below 10 the data cross over the viscous-layer prediction. A similar behavior is observed in the 9° cone data[17] and the present 10° data. However, since the effect of transverse curvature on heat transfer is smaller for the 9° and

10° cones than for the 5° and 6.3° cones, the value of $\bar{\chi}$ at which the departure occurs is not as readily determined. The heat transfer data for the 20° cone appear to follow the transverse-curvature prediction down to $\bar{\chi} = 1.0$; however, for this cone the experimental data remain above the viscous-layer prediction. It appears that the departure from the transverse-curvature prediction occurs at larger values of the rarefaction parameter $\bar{\chi}$ (higher Reynolds numbers) for smaller cone angles.

Although the pressure is not replotted as a function of $\bar{\chi}$, it can be seen from Figure 3 that for the 20° cone the pressure does not greatly exceed the Newtonian value. In the viscous-layer analysis for nonslender cones it is assumed that the pressure is constant and is given by the Newtonian value based on shock angle; the pressure data for the 20° cone thus indicate that this assumption is reasonable. The data presented for the more slender cones[17] show a more significant increase above the Newtonian value; however, they do appear to fall slightly below the interaction prediction for the larger values of $\frac{M_\infty}{\sin^2\theta_c}\sqrt{\frac{C_*}{Re_{x_\infty}}}$ (i.e., for increasing rarefaction). These data appear consistent with the heat transfer, since in this range of $\bar{\chi}$ the heat transfer is only slightly influenced by shock transport.

Both the heat transfer and pressure data appear to support the predictions of the viscous-layer analysis implying that in the viscous-layer regime the effects of slenderness are small, particularly as they influence heat transfer and pressure. However, when separate viscid and inviscid layers exist, slenderness has a more significant effect causing an increase in heat transfer and pressure above the classical boundary-layer limit. In the viscous-layer regime for small $\bar{\chi}$, however, the heat transfer is less than the classical boundary-layer limit even for cone angles as small as 5°.

The viscous-layer analysis is based on the assumptions of a strong shock, and of a thin shock layer. This requires that

$$\epsilon \ll 1 \qquad \frac{1}{\gamma M_\infty^2 \sin^2\beta} \ll 1 \qquad \frac{\delta_s}{r_0} \ll 1$$

For the present experiments these conditions are only partially satisfied. For all the data, $\epsilon \simeq \frac{1}{7}$ and $1/(\gamma M_\infty^2 \sin^2\theta_c)$ is very small except for the 5° cone where its value is about 0.2. The thickness of the shock layer cannot be determined from the available experimental data; however, it is calculated in the Appendix from the nonslender-cone viscous-layer solution at $\bar{x} = 0.1$ to be $\delta_s/r_o \simeq 0.4$ for $\theta_c = 20°$ and to be $\delta_s/r_o \simeq 1.2$ for $\theta_c = 10°$. Thus, although the strong shock assumptions are reasonably satisfied for the present experiments, the thin shock-layer assumption is not.

4.3 Viscous-Layer Regime Incorporating Effects of Slenderness

The results just presented imply that the net effect of slenderness in the viscous-layer regime is small. Thus it would appear that a perturbation analysis could be used to evaluate the effects of slenderness and to yield an improvement in the data correlation. In the Appendix, a perturbation analysis is presented where the zero-order solution is taken as $\bar{u}_o = \alpha_o \zeta$ (the nonslender cone solution for small $\bar{x}$). In this analysis the effects of transverse curvature, viscous-layer displacement and shock curvature are treated as higher order terms and are evaluated from the zero-order velocity. Analytical expressions are obtained for the velocity and enthalpy profiles including the effects of surface slip. The solution assumes a strong shock wave, $\epsilon \ll 1$ and $1/(\gamma M_\infty^2 \sin^2\beta) \ll 1$ and neglects terms of order $\epsilon^2/\sin\beta$. Further discussion of this solution is given in the Appendix as well as graphs of the velocity profiles (Figure A-1), shock angles and shock-layer thickness (Figure A-2) for $\theta_c = 20°$ and 10°.

Surface heat transfer and pressure distribution, as predicted by the perturbation analysis, are compared with the nonslender-cone viscous-layer analysis and the present experimental data in Figure 5. The influence of surface slip on heat transfer is also shown and is seen to be small. For = 20°, the pressure prediction of the perturbation analysis rises above

the Newtonian value and lies slightly below the experimental data. However, the large pressure rise predicted by the Probstein and Elliot interaction analysis is not obtained. For $\theta_c = 20°$, the heat transfer prediction of the perturbation analysis falls above the nonslender-cone prediction, and exhibits a slower rise with increasing rarefaction than the transverse-curvature analysis. The perturbation analysis is in excellent agreement with the experimental data. The heat transfer prediction is also compared with the nonslender-cone solution and the experimental data for $\theta_c = 10°$ in Figure 5. For this case also, good agreement is obtained with the experimental data except for $\bar{\varkappa} < 0.2$. Below this value of $\bar{\varkappa}$ the perturbation solution predicts an increase in $C_H / \sin \theta_c$ with decreasing $\bar{\varkappa}$, whereas the experimental values remain almost constant. Since $C_H / \sin \theta_c \propto \left(\frac{\sin\beta}{\sin\theta_c}\right)^2$ the rise in the theoretical prediction of heat transfer may be due to a small overestimate of the shock angle at and below this value of $\bar{\varkappa}$. The calculations for $C_H / \sin \theta_c$ are not carried beyond $\bar{\varkappa} = 3.0$ since at higher values the perturbed velocity becomes large compared to the zero-order value. A comparison is not given for the 5° cone since for this case the shock layer becomes very thick and the perturbation velocity is no longer small compared to the zero-order value.

It is noted that for the 20° cone, both the experimental data and the perturbation analysis give a value of $C_H / \sin \theta_c$ above the nonslender-cone prediction, whereas, for the 10° cone, the value of $C_H / \sin \theta_c$ predicted by the perturbation analysis lies below the nonslender cone theory (except for the case of $\bar{\varkappa} \simeq 0.20$). This behavior is not too surprising since the effect of slenderness in modifying the nonslender-cone prediction occurs at a higher value of $\bar{\varkappa}$ and thus at a lower value of $C_H / \sin \theta_c$ for the more slender cone.

An examination of the perturbation solution in the Appendix reveals that the transverse curvature is the most dominant of the higher order terms

considered. However, transverse curvature affects both the $\bar{\varkappa}$ momentum differential equation as well as the shock boundary conditions yielding only a small net effect.

5. CONCLUSIONS

The surface heat transfer and pressure data presented in this paper on 5°, 10°, and 20° half-angle cones cover a range of Mach numbers from 19 to 24 and Reynolds numbers per inch from 150 to 4000. The large rise in heat transfer and pressure predicted by previous studies of transverse curvature[5] of and boundary-layer displacement[4] is not observed experimentally even for the 5° cone. The experimental data expressed as $C_H / \sin \theta_c$ and $(p/p_\infty)/\gamma M_\infty^2 \sin^2 \theta_c$ exhibit only a small dependence on cone angle and are in close agreement with Cheng's viscous-layer analysis for nonslender cones.[1] This agreement implies that the effects of cone slenderness on heat transfer and pressure in the viscous-layer regime are small. As the cone angle decreases the experimental data on heat transfer (obtained from both the current study and Reference 17) merge into the predictions of the transverse-curvature analysis, based on separate viscous and inviscid layers, at higher values of the rarefaction parameter $\bar{\varkappa}$ (i.e., higher Reynolds numbers). This trend is particularly obvious from the data for the 20° and 6.3° cones.

The relative importance of the parameters associated with decreasing cone angle is examined by obtaining a perturbation solution of the differential equation governing momentum where an analytical form of the viscous-layer nonslender-cone solution of Cheng[1] is used as the zero-order term. The perturbation solution includes the effect of shock curvature, shock angle not equal to cone angle, viscous-layer displacement and transverse curvature. This solution reveals that transverse curvature is a dominant phenomenon in controlling the velocity and enthalpy profiles. However, the net effect of the

transverse curvature term retained both in the shock boundary conditions and in the differential equation is small. The prediction of both surface pressure and heat transfer from the perturbation solution yields improved agreement with the experimental data. The effect of surface slip and temperature jump has been examined for the case of a cold wall and an expression obtained for correction of heat transfer due to slip effects in terms of the no-slip solution. For the present experimental conditions this correction is small.

The present study reveals the importance of transport at the shock in reducing heat transfer below the classical boundary-layer limit. This result is valid even for relatively slender cones where transverse curvature is present. Also the present results suggest a wider range of applicability of Cheng's viscous-layer model and of his solution for nonslender cones than would be inferred by the assumptions inherent in the analysis, particularly as regards the thin shock-layer assumption.

REFERENCES

1. Cheng, H.K., "The Blunt-Body Problem in Hypersonic Flow at Low Reynolds Number," CAL Report No. AF-1285-A-10 (June 1963).

2. Vidal, R.J. and Bartz, J.A., "Experimental Studies of Low-Density Effects in Hypersonic Wedge Flows," AFOSR 65-0335, CAL Report No. AF-1500-A-2 (December 1964).

3. Vidal, R.J. and Wittliff, C.E., "Hypersonic Low-Density Studies of Blunt and Slender Bodies," Rarefied Gas Dynamics Third Symposium, Vol II (Ed. J.A. Laurmann), Academic Press (1963).

4. Probstein, R.F., "Interacting Hypersonic Laminar Boundary Layer Flow Over a Cone," Div. Eng., Brown Univ. Tech. Report AF-2798/1 (March 1955).

5. Probstein, R.F. and Elliot, E., "The Transverse Curvature Effect in Compressible Axially Symmetric Laminar-Boundary-Layer Flow," J. Aero. Sci. 28, 3 (1956).

6. Talbot, L., Koga, T., and Sherman, P.M. "Hypersonic Viscous Flow Over Pointed Cones," NACA TN 4327 (1958).

7. Lewis, C.H. and Whitfield, J.D., "Theoretical and Experimental Studies of Hypersonic Viscous Effects," AEDC TR 65-100 (May 1965).

8. Yasuhara, N., "Axisymmetric Viscous Flow Past Very Slender Bodies of Revolution," J. Aero-Space Sci. 29, 6 (June 1962).

9. Stewartson, K., "Viscous Hypersonic Flow Past a Slender Cone," Physics of Fl., 7, 5 (May 1964).

10. Hilton, J.H., Golian, T.C., Somers, L.M., Wilson, M.R., and Fabian, G.J., "Development and Performance of the CAL Six-Foot Hypersonic Shock Tunnel," CAL Report No. CAL-120 (January 1966).

11. Eschenroeder, A.Q., Boyer, D.W., and Hall, J.G., "Nonequilibrium Expansions of Air with Coupled Chemical Reactions," Phys. Fluids 5, 5, pp. 615-624 (May 1962) (See also CAL Report No. AF-1413-A-1, May 1961).

12. Vidal, R.J., "Transient Surface Temperature Measurements," CAL Report No. CAL-114 (March 1962).

13. Skinner, G.T., "Analog Network to Convert Surface Temperature to Heat Flux," CAL Report No. CAL-100 (February 1960); also ARS J. 30, 6 (June 1960).

14. Hayes, W.D. and Probstein, R.F., "Hypersonic Flow Theory," Academic Press (1959).

15 Cheng, H.K. and Cheng, A.L., "Stagnation Region in Rarefield High Mach Number Flow," AIAA J. 1, 1 (1963).

16. Cheng, H.K., "Hypersonic Flow with Combined Leading-Edge Bluntness and Boundary-Layer Displacement Effect," CAL Report No. 1285-A-4 (August 1960).

17. Wilkinson, D.B. and Harrington, S.A., "Hypersonic Force Pressure and Heat Transfer Investigations of Sharp and Blunt Slender Cones," AEDC TDR 63-177 (August 1963).

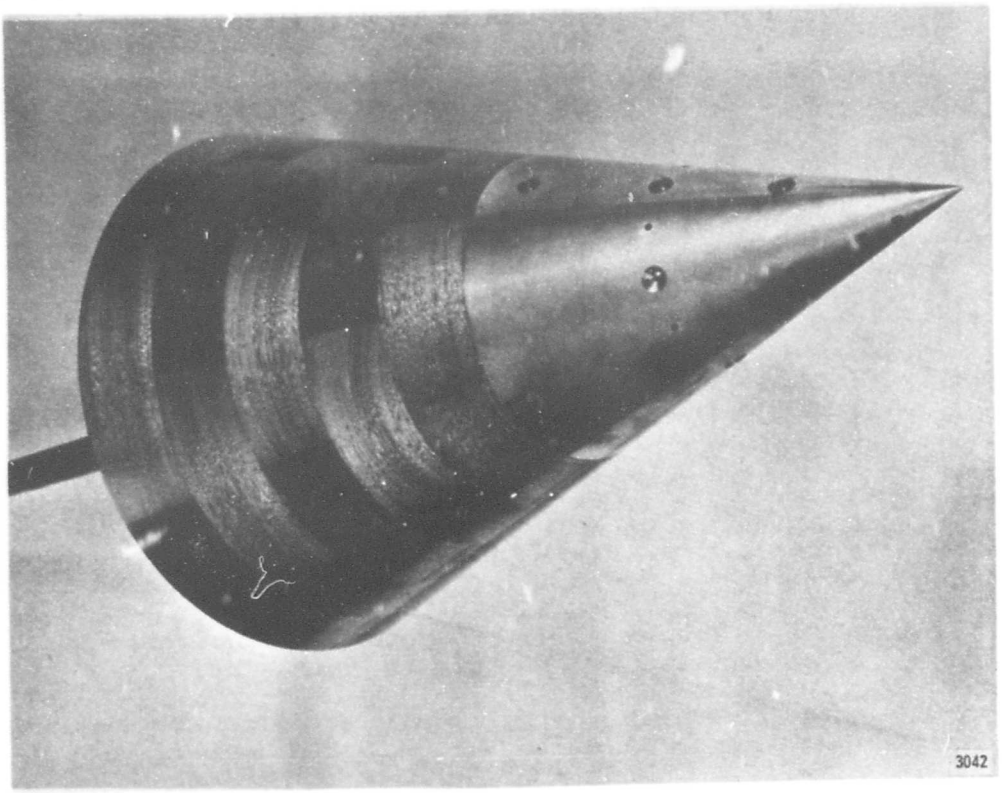

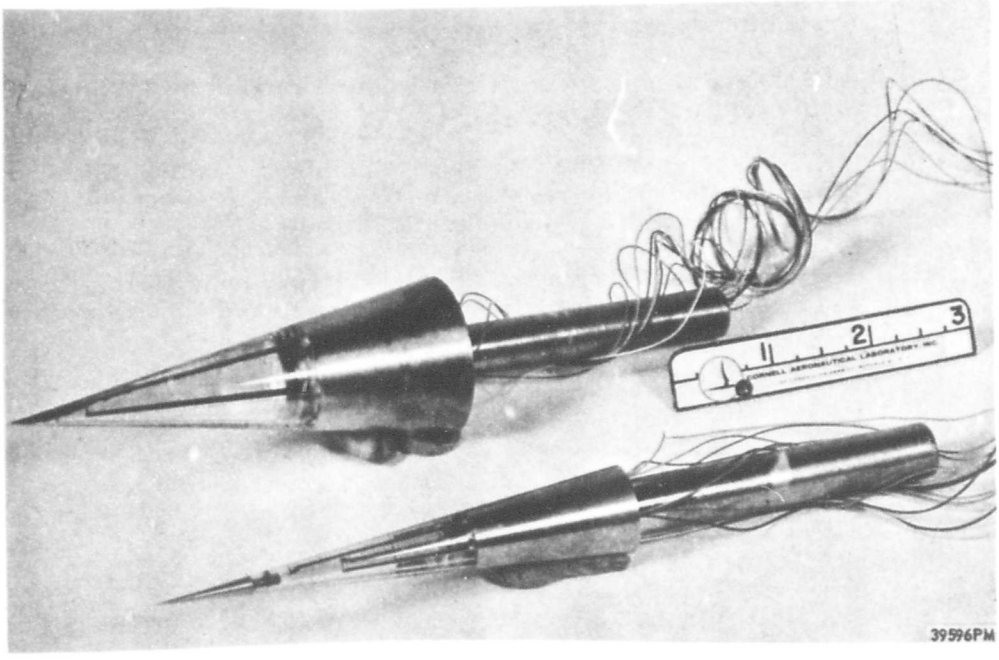

Figure 1 10°, 20° AND 40° TOTAL ANGLE CONE MODELS

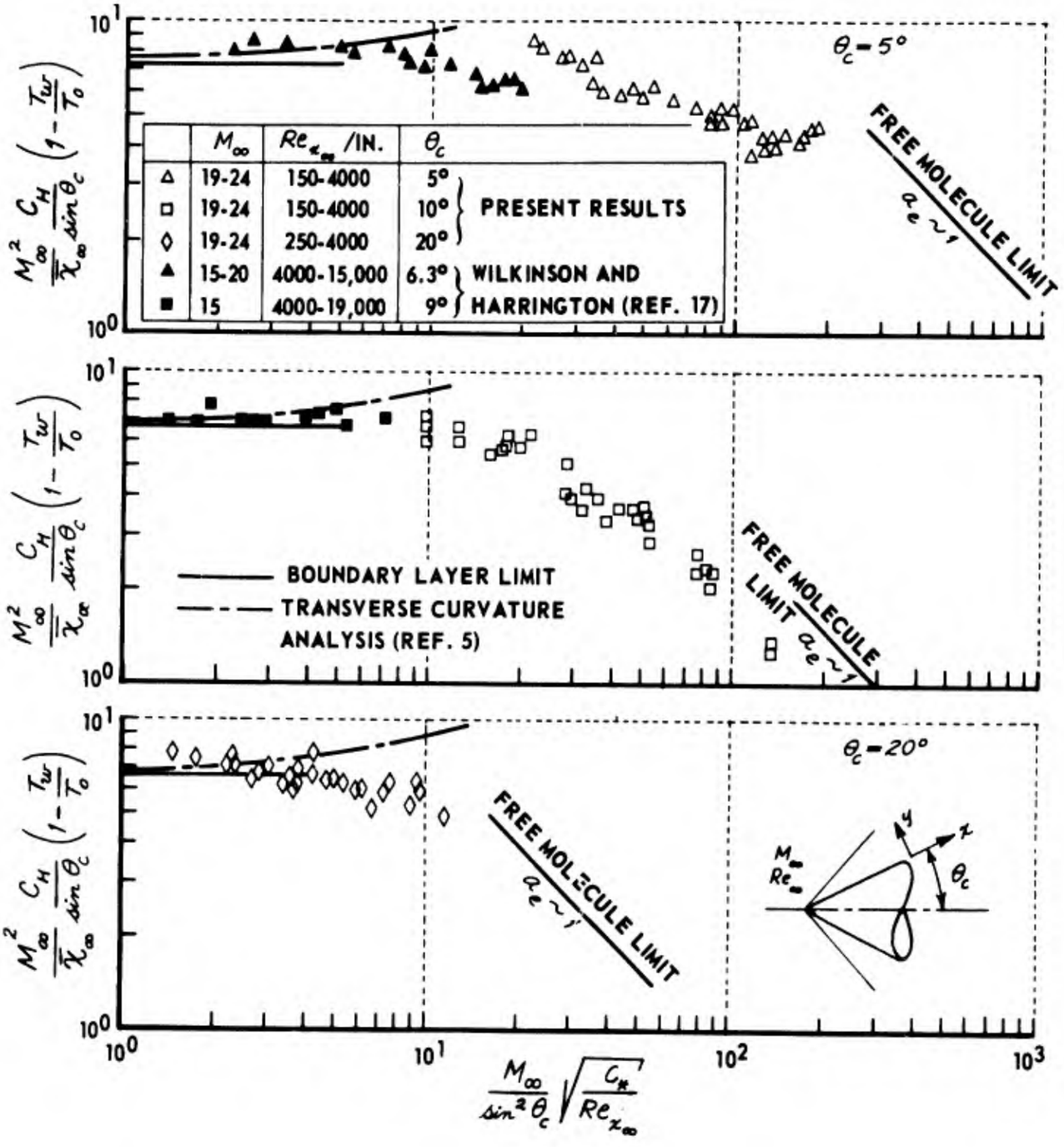

Figure 2 COMPARISON OF CONE HEAT TRANSFER DATA WITH PREDICTIONS OF A VISCOUS-INVISCID INTERACTION ANALYSIS INCLUDING TRANSVERSE CURVATURE

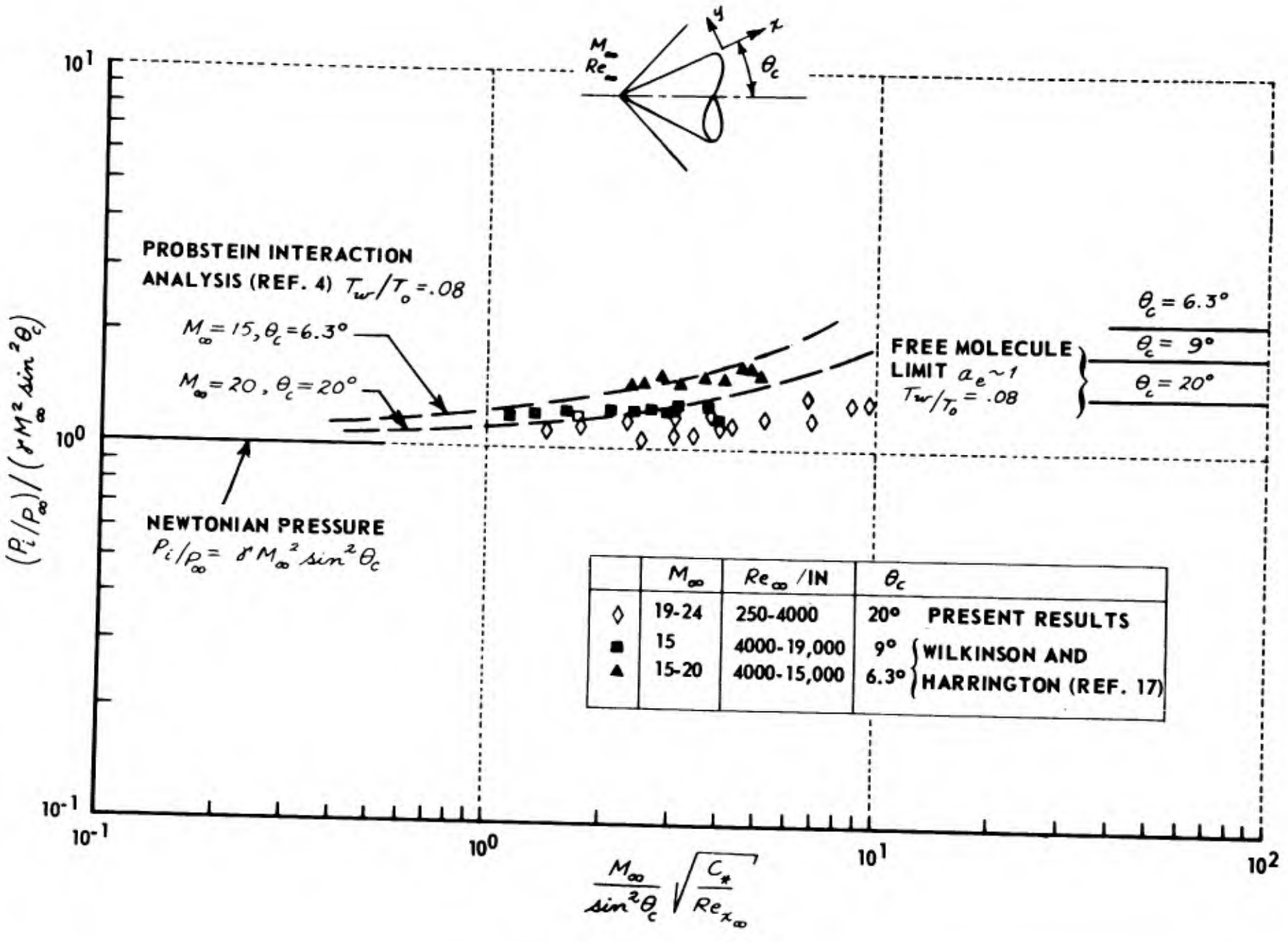

Figure 3 CONE PRESSURE DATA

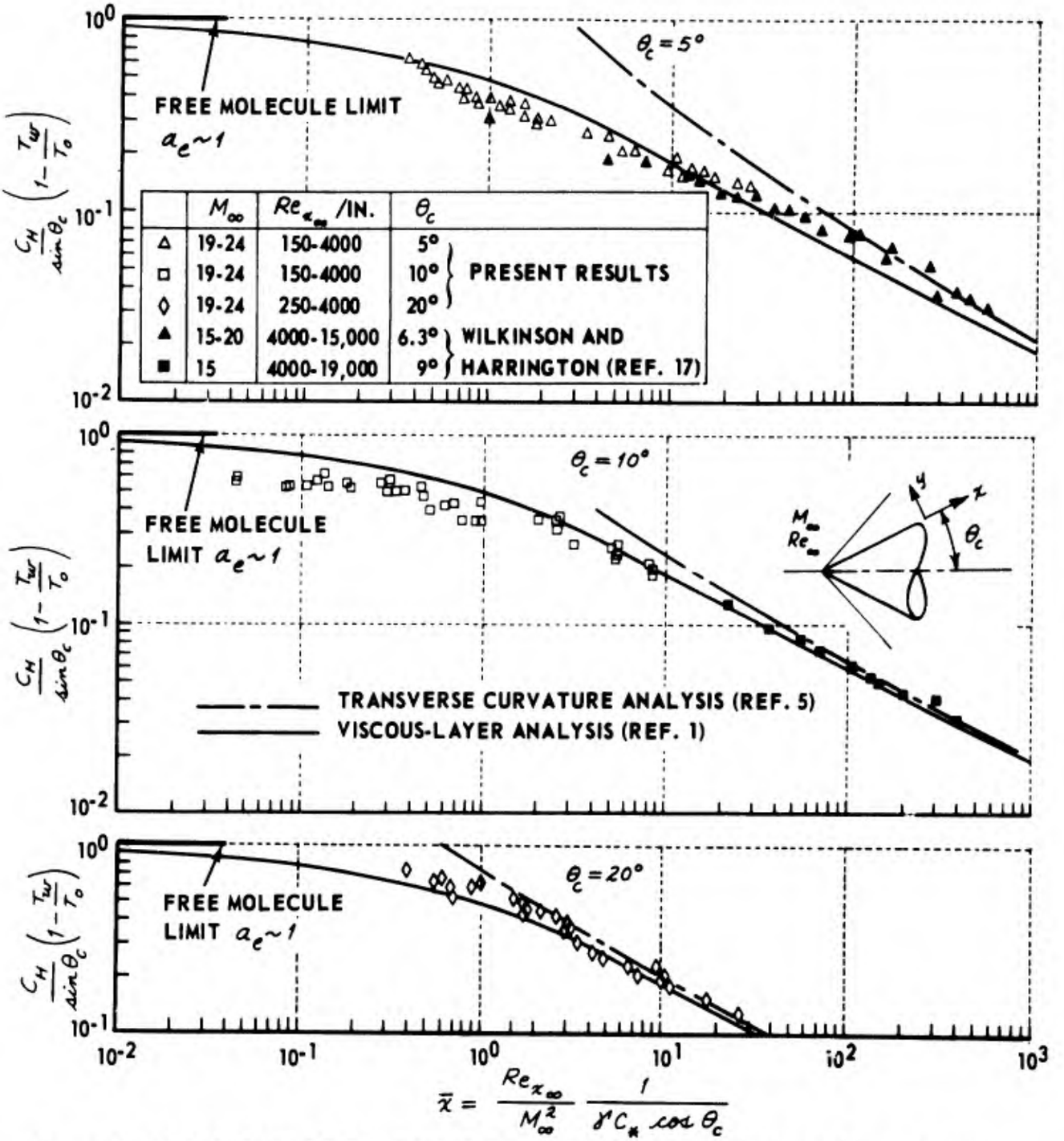

Figure 4 COMPARISON OF CONE HEAT TRANSFER WITH VISCOUS LAYER ANALYSIS

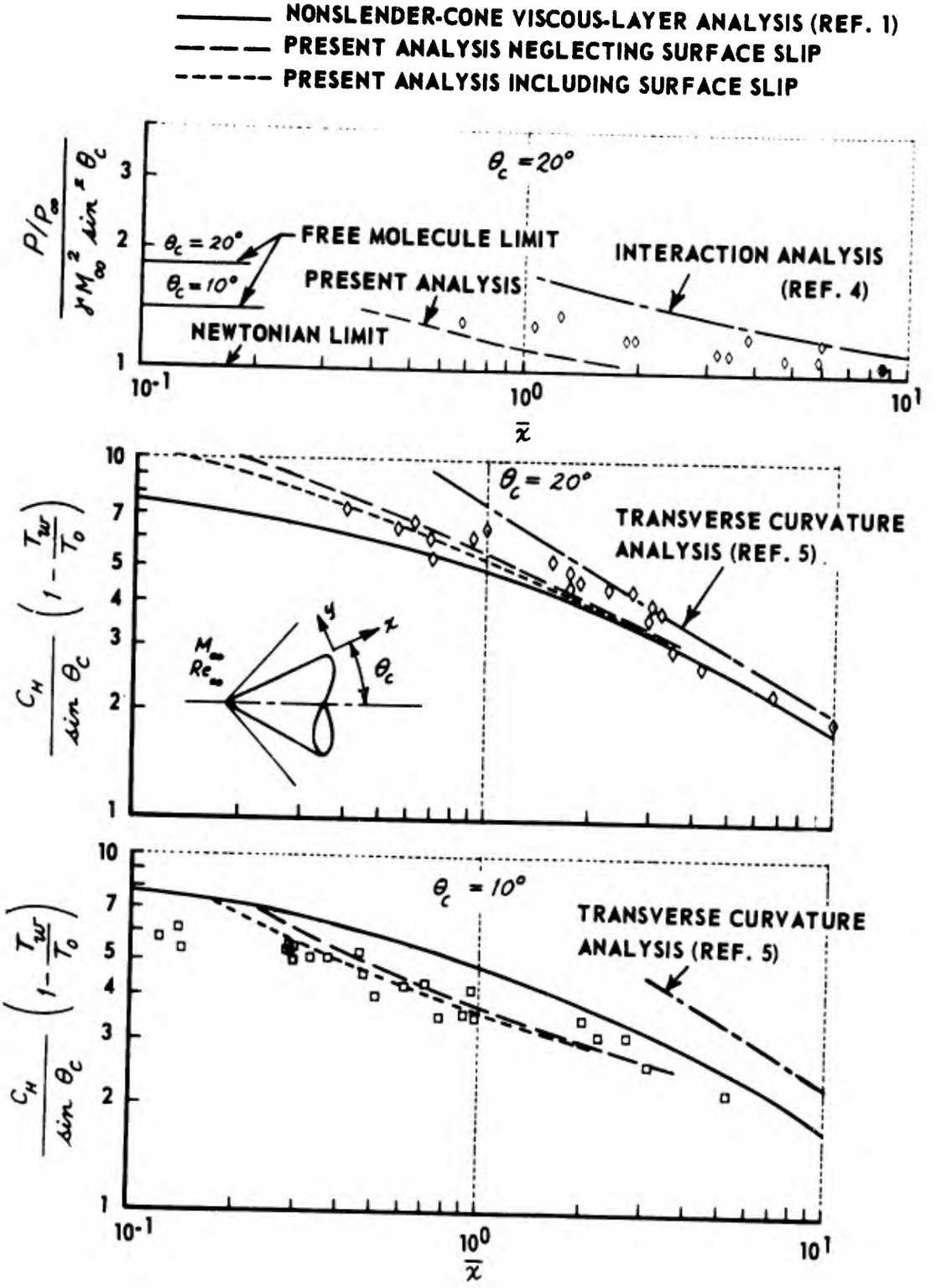

Figure 5 COMPARISON OF THEORETICAL AND EXPERIMENTAL HEAT TRANSFER AND PRESSURE

7. APPENDIX

EXTENSION OF CHENG'S VISCOUS-LAYER ANALYSIS TO NOT-TOO-SLENDER CONES

Basic Equations

Under the assumptions that the specific heat ratio is constant, Prandtl number is unity, body forces are negligible and the gas obeys the perfect gas law, the axially symmetric boundary-layer equations may be written as follows (after the usual order of magnitude analysis)

continuity $$\frac{\partial}{\partial x}(\rho u r) + \frac{\partial}{\partial y}(\rho v r) = 0$$

x momentum $$\frac{\partial p}{\partial x} + \rho u \frac{\partial u}{\partial x} + \rho v \frac{\partial u}{\partial y} = \frac{1}{r}\frac{\partial}{\partial y}\left(r\mu \frac{\partial u}{\partial y}\right) \qquad \text{A-1(a)}$$

y momentum $$\frac{\partial p}{\partial y} + \rho u \frac{\partial v}{\partial x} + \rho v \frac{\partial v}{\partial y} = 0$$

energy $$\rho u \frac{\partial H}{\partial x} + \rho v \frac{\partial H}{\partial y} = \frac{1}{r}\frac{\partial}{\partial y}\left(r\mu \frac{\partial H}{\partial y}\right)$$

These equations include the transverse-curvature effect $r = r(x,y)$ and the viscous-layer displacement. The equations are identical to those solved by Probstein[4] and Yasuhara[8] except that, in their study, $\frac{\partial p}{\partial y} = 0$. The boundary conditions at the shock are obtained by solving the equations of motion across the shock transition zone under the assumptions that

$$\theta(\epsilon) \leq \frac{v}{u_\infty \sin\beta} \leq 1 \qquad \text{and} \qquad \frac{\partial}{\partial x} \ll \frac{\partial}{\partial y}$$

in a manner similar to that employed for the nonslender cone case. The equations of motion across the shock transition zone reduce to

$$\frac{\partial}{\partial y}(\rho v) - (\beta - \theta_c)\frac{\partial}{\partial y}(\rho u) = 0$$

$$\rho v \frac{\partial u}{\partial y} - (\beta - \theta_c)\rho u \frac{\partial u}{\partial y} = \frac{\partial}{\partial y}\left(\mu \frac{\partial u}{\partial y}\right) \qquad \text{A-1(b)}$$

$$\frac{\partial p}{\partial y} + \left[\rho v - (\beta - \theta_c)\rho u\right]\left[\frac{\partial v}{\partial y} - (\beta - \theta_c)\frac{\partial u}{\partial y}\right] = 0$$

$$\left[\rho v - (\beta - \theta_c)\rho u\right]\frac{\partial H}{\partial y} = \frac{\partial}{\partial y}\left(\mu \frac{\partial H}{\partial y}\right)$$

In Equations A-1(b), the reference surface is taken as the body rather than as the shock as in the nonslender cone study.[1] These equations may be directly integrated and the free-stream conditions used to determine the constants of integration. Thus, Equations A-1 (b) reduce to

$$v_s = -\epsilon u_\infty \sin\beta + (\beta - \theta_c)u$$

$$u_s = u_\infty \cos\beta - \left(\mu \frac{\partial u}{\partial y}\right)_s \Big/ \rho_\infty u_\infty \sin\beta \qquad \text{A-2}$$

$$p_s = \rho_\infty u_\infty \sin^2\beta\,(1 - \epsilon)$$

$$H_s = H_\infty - \left(\mu \frac{\partial H}{\partial y}\right)_{y=0} \Big/ \rho_\infty u_\infty \sin\beta$$

where the subscript s refers to conditions behind the shock and the strong shock approximations are made (i.e., $p_\infty \ll p_s$ and $1/(\gamma M_\infty^2 \sin^2\beta) \ll 1$). These boundary conditions represent a set of modified Rankine-Hugoniot conditions similar to those developed for the nonslender cone.

Equations A-1(a) may be expressed in terms of the dimensionless quantities $\bar{u}, \bar{v}, \bar{p}$ and Θ and the independent variables $\bar{x}$ and ζ as introduced by Cheng.[1]

$$\bar{u} = \frac{u}{u_\infty \cos\beta} \qquad \bar{v} = \frac{v}{\epsilon u_\infty \sin\beta}$$

$$\bar{p} = \frac{p}{\rho_\infty u_\infty^2 \sin^2\beta} \qquad \Theta = \frac{H - H_w}{H_\infty - H_w} \qquad \text{A-3}$$

$$\zeta^2 = \frac{\psi}{\rho_\infty u_\infty \pi r^2} \qquad \bar{x} = \frac{\epsilon \rho_\infty u_\infty x \sec\beta}{\mu_0}\left(\frac{\mu_0}{\mu_*}\frac{T_*}{T_0}\right)$$

where ψ is the stream-tube coordinate defined by

$$\left(\frac{\partial \psi}{\partial y}\right)_x = 2\pi r \rho u$$

The transformation to $\bar{x}$, ζ coordinates is accomplished through the following

$$\left(\frac{\partial}{\partial x}\right)_y = \left(\frac{\partial}{\partial x}\right)_\psi - 2\pi r \rho v \left(\frac{\partial}{\partial \psi}\right)_x$$

$$\left(\frac{\partial}{\partial y}\right)_x = 2\pi r \rho u \left(\frac{\partial}{\partial \psi}\right)_x$$

and

$$\left(\frac{\partial}{\partial x}\right)_\psi = \frac{\bar{x}}{x}\left(\frac{\partial}{\partial \bar{x}}\right)_\zeta - \frac{\zeta}{r}\sin\theta_c \left(\frac{\partial}{\partial \zeta}\right)_{\bar{x}}$$

$$\left(\frac{\partial}{\partial \psi}\right)_x = \frac{(1-\varphi)}{2\zeta \rho_\infty u_\infty \pi r^2}\left(\frac{\partial}{\partial \zeta}\right)_{\bar{x}}$$

where $\varphi = 2\pi r \rho_\infty u_\infty \zeta^2 \left(\frac{\partial r}{\partial \psi}\right)_x$

Under these transformations, the continuity equation is automatically satisfied and the x momentum and enthalpy equations are reduced to

$$\bar{x}\bar{u}\frac{\partial \bar{u}}{\partial \bar{x}} = \frac{r_0}{r}\zeta\bar{u}\frac{\partial \bar{u}}{\partial \zeta} + \left(\frac{r_0}{r}\right)^2 \frac{\sin^2\beta}{\sin^2\theta_c}\frac{\bar{u}}{\zeta\bar{x}}(1-\varphi)\frac{\partial}{\partial \zeta}\left[\frac{\bar{\rho}\bar{u}}{\zeta}(1-\varphi)\frac{\partial \bar{u}}{\partial \zeta}\right]$$

$$-\frac{2\epsilon\bar{x}}{\cos^2\theta_c}\frac{T}{T_0}\cot\theta_c\frac{\partial \beta}{\partial \bar{x}} \qquad \text{A-4(a)}$$

$$\bar{x}\frac{\partial \Theta}{\partial \bar{x}} = \zeta\frac{r_0}{r}\frac{\partial \Theta}{\partial \zeta} + \left(\frac{r_0}{r}\right)^2 \frac{\sin^2\beta}{\sin^2\theta_c}\frac{(1-\varphi)}{\zeta\bar{x}}\frac{\partial}{\partial \zeta}\left[\frac{\rho\bar{u}}{\zeta}(1-\varphi)\frac{\partial \Theta}{\partial \zeta}\right]$$

where small terms have been neglected.

The shock boundary conditions are:

$$\bar{u} = 1 - \frac{r_0}{r_s}\,\frac{\sin\beta}{\sin\theta_c}\,\frac{\bar{p}_s}{\bar{x}}\,(1-\varphi_s)\left(\bar{u}\,\frac{\partial \bar{u}}{\partial \zeta}\right)_{\zeta=1}$$

$$\Theta = 1 - \frac{r_0}{r_s}\,\frac{\sin\beta}{\sin\theta_c}\,\frac{\bar{p}_s}{\bar{x}}\,(1-\varphi_s)\left(\bar{u}\,\frac{\partial \Theta}{\partial \zeta}\right)_{\zeta=1} \qquad \text{A-4 (b)}$$

In the above equations, a linear viscosity temperature relation is assumed, based on the reference temperature T_* .

Solution for the Perturbed Flow Field

Utilizing as the zero-order solution the nonslender-cone solution given in the form $\bar{u}_0 = \alpha_0 \zeta$ as discussed in Section 2.2, the values $\frac{r}{r_0}$, $\frac{\partial \beta}{\partial \bar{x}}$, $\frac{\sin\beta}{\sin\theta_c}$ and $\bar{p}$ may be determined. From the definition of the stream tube function,

$$\frac{\partial \psi}{\partial y} = 2\pi r \rho u = \frac{2\pi r \rho_\infty u_\infty \sin^2\theta_c \cos\theta_c}{\epsilon(1-\bar{u}_0\cos^2\theta_c)}$$

the value of r/r_0 is determined as:

$$\left(\frac{r}{r_0}\right)^2 = 1 + \frac{\epsilon\zeta^2}{\sin^2\theta_c}\left(1 - \frac{2}{3}\alpha_0\zeta\cos^2\theta_c\right) \qquad \text{A-5}$$

By defining $(\beta-\theta_c) = \frac{dy_s}{dx}$ where y_s is the shock coordinate, the value of $(\beta-\theta_c)$ is determined as:

$$(\beta-\theta_c) = \left(\frac{r_s}{r_0} - 1\right)\tan\theta_c - \frac{r_0}{r_s}\,\frac{\epsilon\bar{x}\cot\theta_c}{3}\,\frac{\partial \alpha_0}{\partial \bar{x}} \qquad \text{A-6}$$

and $\frac{\sin\beta}{\sin\theta_c} = 1 + (\beta-\theta_c)\cot\theta_c$ for $\sin(\beta-\theta_c) \simeq (\beta-\theta_c)$.

The y-momentum equation, given as the third equation in Equations A-1(a), can be represented by:[14]

$$\frac{\partial p}{\partial y} \simeq \frac{\rho u^2}{R} \qquad \text{A-7}$$

where R is the radius of curvature of the streamlines and is given by

$$R^{-1} \simeq \frac{\partial^2 y}{\partial x^2}$$

In the nondimensionalized form, Equation A-7 can be written as

$$\frac{\partial \bar{p}}{\partial \zeta} = \alpha_0 \zeta^2 \left[1 - \left(\frac{r_0}{r}\right)^2\right]$$

or applying the shock boundary condition $\bar{p}(1) = 1 - \epsilon$

$$\bar{p} = 1 - \epsilon - \alpha_0 \int_{\zeta}^{1} \zeta^2 \left[1 - \left(\frac{r_0}{r}\right)^2\right] d\zeta \qquad \text{A-8}$$

In the derivation of $\partial \bar{p}/\partial \zeta$, the variation of α_0 with $\bar{x}$ is determined from the zero-order differential equation as

$$\frac{\partial \alpha_0}{\partial \bar{x}} = \frac{\alpha_0}{\bar{x}}$$

Since the departure from the linear form of $\bar{u}_0 = \alpha_0 \zeta$ has been determined by Cheng from the numerical solution to occur at the shock wave for $\bar{x} \geq 1$ the numerical value of $\partial \alpha_0 / \partial \bar{x}$ is retained in the numerical determination of $(\beta - \theta_c)$. To the order of the present analysis, however, the value of $\bar{p}$ is adequately represented by Equation A-8.

Equations A-5, A-6, and A-8 now define the higher order terms (except for slip effects) neglected by Cheng in the nonslender-cone analysis in terms of the assumed zero-order solution. These results may be used to further simplify the x-momentum given as the first of Equations A-4 (a) where the coefficients of $\frac{\partial}{\partial \zeta}\left(\frac{\bar{u}}{\zeta}\frac{\partial \bar{u}}{\partial \zeta}\right)$, $\frac{\partial \bar{p}}{\partial \zeta}$ and $\frac{\partial \varphi}{\partial \zeta}$ terms are expressed by the zero-order solution; that is, $r \simeq r_0$, $\beta \simeq \theta_c$, $\varphi \simeq 0$ and $\bar{u} \simeq \alpha_0 \zeta$. Also

it is assumed that the variation of $\bar{u}$ with $\bar{x}$ is given by the zero-order solution. Substituting $\bar{u} = \sqrt{2W}$, the x-momentum equation may be reduced to

$$\bar{x}\frac{\partial W}{\partial \bar{x}} = \zeta \frac{r_o}{r}\frac{\partial W}{\partial \zeta} + \frac{\alpha_o}{\bar{x}}\frac{\partial}{\partial \zeta}\left(\frac{1}{\zeta}\frac{\partial W}{\partial \zeta}\right) + \frac{\alpha_o^3}{\bar{x}}\left(\frac{\partial \bar{p}}{\partial \zeta} - \frac{\partial \varphi}{\partial \zeta}\right)$$

$$- \frac{2\epsilon \bar{x}}{\cos^2\theta_c}\,\alpha_o \zeta\left(1 - \alpha_o \zeta \cos^2\theta_c\right)\cot\beta\,\frac{\partial \beta}{\partial \bar{x}} \qquad \text{A-9}$$

Letting $W = W_o + W_1$ (where W_o is the zero order term $\frac{\alpha_o^2 \zeta^2}{2}$ and W_1 is the perturbed velocity term) and neglecting small terms $\frac{W_1}{W_o} \ll 1$, the following differential equation in W_1 is obtained

$$\frac{\partial^2 W_1}{\partial \zeta^2} + \frac{\partial W_1}{\partial \zeta}\left(\frac{\bar{x}\zeta^2}{\alpha_o} - \frac{1}{\zeta}\right) = Q(\bar{x}, \zeta) \qquad \text{A-10}$$

where

$$Q(\bar{x}, \zeta) = \alpha_o \bar{x} \zeta^3\left(1 - \frac{r_o}{r}\right) - \alpha_o^2 \zeta\left(\frac{\partial \bar{p}}{\partial \zeta} - \frac{\partial \varphi}{\partial \zeta}\right)$$

$$+ \frac{2\epsilon \bar{x}^2 \zeta^2}{\cos^2\theta_c}\left(1 - \alpha_o \zeta \cos^2\theta_c\right)\cot\theta_c\,\frac{\partial \beta}{\partial \bar{x}} \qquad \text{A-10 (a)}$$

The solution of Equation A-10 is given by

$$\frac{\partial W_1}{\partial \zeta} \simeq A\zeta\left(1 - \frac{\bar{x}\zeta^3}{3\alpha_o}\right) + \zeta\int_0^\zeta \frac{1}{\zeta}\,Q(\bar{x}, \zeta)\,d\zeta \qquad \text{A-11}$$

$$W_1 = \frac{A\zeta^2}{2}\left(1 - \frac{2\bar{x}\zeta^3}{15\alpha_o}\right) + \int_0^\zeta \zeta\left[\int_0^\zeta \frac{Q(\bar{x}, \zeta)}{\zeta}\,d\zeta\right]d\zeta + B$$

where A and B are determined from the boundary conditions at the shock and the wall, respectively. For the case of zero slip at the wall

$$W_1(0) = 0 \qquad \text{and} \qquad B = 0.$$

The boundary condition at the shock is

$$W_1(1) \simeq \frac{\alpha_o^3}{\bar{x}}\left[1 - \frac{r_o}{r_s}\frac{\sin\beta}{\sin\theta_c}\,\bar{p}_s\left(1 - \varphi_s\right)\right] - \frac{\alpha_o}{\bar{x}}\left(\frac{\partial W_1}{\partial \zeta}\right)_{\zeta=1}$$

from which

$$\frac{A}{2\alpha_0^2}\left(\frac{1}{6}+\frac{\alpha_0}{\bar{x}}-\frac{\bar{x}}{15\alpha_0}\right)=\frac{\alpha_0}{2\bar{x}}\left[1-\frac{r_0}{r_s}\frac{\sin\beta}{\sin\theta_c}\bar{p}_s\left(1-\varphi_s\right)\right]$$

$$-\frac{1}{2\alpha_0}\sum_n\frac{a_n}{n+2}\left[1+\frac{\alpha_0}{\bar{x}}(n+2)\right] \qquad \text{A-12}$$

where

$$\int_0^\zeta\frac{Q(\bar{x},\zeta)}{\alpha_0\zeta}\,d\zeta=\sum_n a_n\zeta^n \qquad \text{A-12(a)}$$

Only a_2 and a_3 have a non-negligible contribution and are given by

$$a_2=\frac{\epsilon\alpha_0}{\sin^2\theta_c} \qquad a_3=-\epsilon\alpha_0^2\cot^2\theta_c \qquad \text{A-12(b)}$$

These two terms are due solely to the expansion of φ, the transverse curvature parameter. Thus, this yields, for the velocity flow field,

$$\bar{u}\simeq\alpha_0\zeta\left(1+\frac{W_1}{\alpha_0^2\zeta^2}\right)$$

$$\simeq\alpha_0\zeta\left[1+\frac{A}{2\alpha_0^2}\left(1-\frac{2\bar{x}\zeta^3}{15\alpha_0}\right)+\frac{\epsilon\zeta^2}{4\sin^2\theta_c}-\frac{\epsilon\alpha_0\cot^2\theta_c\,\zeta^3}{5}\right] \qquad \text{A-13)}$$

This expression for the flow field now includes the effects of transverse curvature and shock angle not equal to body angle; the viscous-layer displacement effects are small and have been neglected in the coefficients a_2 and a_3 given in Equation A-12(b). The enthalpy equation given by the second Equation A-4(a) is satisfied by $\bar{u}=\theta$.

The heat transfer expressed in terms of the Stanton number is defined as

$$C_H\equiv\frac{c_p\left(\mu\frac{\partial T}{\partial y}\right)_{y=0}}{\rho_\infty u_\infty(H_\infty-H_w)}$$

which, in the present coordinate system, may be expressed as

$$\frac{C_H}{\sin\theta_c} = \left(\frac{\sin\beta}{\sin\theta_c}\right)^2 \frac{\bar{p}_w}{\bar{x}} \left(\frac{\bar{u}}{\zeta}\frac{\partial\Theta}{\partial\zeta}\right)_{\zeta=0} \qquad \text{A-14}$$

In terms of the perturbation solution, the heat transfer is expressed

$$\frac{C_H}{\sin\theta_c} = \left(\frac{\sin\beta}{\sin\theta_c}\right)^2 \frac{\bar{p}_w}{\bar{x}} \alpha_0^2 \left(1 + \frac{A}{2\alpha_0^2}\right)^2 \qquad \text{A-15}$$

Surface Slip Effects

By defining the slip velocity Δu and temperature jump ΔT at the wall as

$$\Delta u \simeq \lambda_s \left(\frac{\partial T}{\partial y}\right)_{y=0} \qquad \text{and} \qquad \Delta T \simeq \lambda_j \left(\frac{\partial T}{\partial y}\right)_{y=0}$$

the surface boundary conditions may be expressed as

$$1 = \bar{\lambda}\left(\frac{1}{\zeta}\frac{\partial\bar{u}}{\partial\zeta}\right)_{\zeta=0} \qquad \Theta(0) = \bar{\lambda}\frac{\lambda_j}{\lambda_s}\left(\frac{\bar{u}}{\zeta}\frac{\partial\Theta}{\partial\zeta}\right)_{\zeta=0}$$

where

$$\bar{\lambda} = \frac{\lambda_s}{\lambda_w}\frac{1}{k_1\bar{x}\sin\beta}\sqrt{\epsilon\frac{T_w}{T_0}}$$

The flow velocity incorporating the higher order effects may be written as

$$\bar{u}_s = \sqrt{\alpha_0^2\zeta^2 + 2W_1 + A_s\zeta^2\left(1 - \frac{2\bar{x}\zeta^3}{15\alpha_0}\right) + 2B_s}$$

where B_s and A_s are the integration constants to be determined from the wall and shock boundary condition, due to the surface slip effects only. The resultant solution for the flow velocity is

$$\bar{u}_s = \sqrt{\alpha_o^2 \zeta^2 + (2W)_{NS} + \alpha_o^4 \bar{\lambda}^2 \left(1 + \frac{A}{2\alpha_o^2}\right)^2 \left[1 - \frac{\zeta^2 (1 - 2\bar{x}\zeta^3/15\alpha_o)}{2(1/6 + \alpha_o/\bar{x} - \bar{x}/15\alpha_o)}\right]} \qquad \text{A-16}$$

The solution for the enthalpy equation incorporating surface slip effects may be written as

$$\Theta_s = \bar{u} + \Theta_1 \qquad \text{A-17}$$

After substituting in the second of Equations A-4 (a) the following differential equation for Θ_1 is obtained.

$$\frac{\partial^2 \Theta_1}{\partial \zeta^2} + \frac{\partial \Theta_1}{\partial \zeta}\left(\frac{\bar{x}\zeta^2}{\alpha_o}\right) = 0$$

for which the solution is

$$\Theta_1 = A_{1_s}\zeta\left(1 - \frac{\bar{x}\zeta^3}{12\alpha_o}\right) + B_{1_s}$$

Applying the enthalpy boundary conditions at the surface and the shock, Θ_{1_s} is determined as:

$$\Theta_{1_s} = \alpha_o^2 \bar{\lambda}\left(1 + \frac{A}{2\alpha_o^2}\right)\left(\frac{\lambda_j}{\lambda_s} - 1\right)\left[1 - \frac{\zeta(1 - \bar{x}\zeta^3/12\alpha_o)}{(2/3 + \alpha_o/\bar{x} - \bar{x}/12\alpha_o)}\right] \qquad \text{A-18}$$

where terms of $\mathcal{O}(\epsilon\alpha_o\bar{\lambda})$ have been neglected. After substituting for $\bar{\lambda}$ and for $\frac{C_H}{\sin\theta_c}$ (Equation A-14), an expression can be obtained for the ratio of heat transfer incorporating slip effects to the heat transfer without slip effects as

$$\frac{(q)_s}{(q)_{NS}} = 1 - \frac{\alpha_o\left(\frac{\lambda_j - \lambda_s}{\lambda_w}\right)\sqrt{\epsilon\frac{T_w}{T_o}}}{k_1 \bar{x}\sin\beta\left(\frac{2}{3} + \frac{\alpha_o}{\bar{x}} - \frac{\bar{x}}{12\alpha_o}\right)} \qquad \text{A-19}$$

This relation is very similar to that developed by Cheng[16] for the heat transfer at the stagnation point of a blunt axisymmetric body, except for the dependence on $\sin\beta\left(\frac{2}{3}+\frac{\alpha_0}{\bar{\varkappa}}-\frac{\bar{\varkappa}}{12\alpha_0}\right)$ and the difference in the rarefaction parameters developed for the cone $(\bar{\varkappa})$ and the blunt body (K^2).

Discussion

The results of this perturbation analysis as regards heat transfer predictions have been presented in Figure 5 and discussed in Section 4.3. Now attention is directed to the perturbed velocity profiles, the shock layer thickness, and the difference between shock angle and body angle.

An examination of Equation A-13 for the velocity field $\bar{u}$ reveals that the dominant effect perturbing $\bar{u}$ from the assumed zero-order linear form is that due to φ, the transverse curvature parameter $(\varphi \propto \partial r/\partial\psi)$. In the present analysis, its effect is included in both the shock boundary conditions and the differential equation governing velocity and enthalpy. The effect of transverse curvature can be seen in Figure A-1, which presents the velocity profiles $\bar{u}(\zeta)$ for $\bar{\varkappa}$ = 0.1, 0.4, 1.0, and 3.0 for cone half-angles θ_c = 10° and 20°. It is observed that transverse curvature increases the velocity near the shock while decreasing it near the body relative to Cheng's solution for a nonslender cone. Also, the velocity increment at the shock increases with decreasing values of the rarefaction parameter $\bar{\varkappa}$ (i.e., as the cone vertex is approached).

At the wall, transverse curvature acts to decrease the velocity gradient $(\partial\bar{u}/\partial\zeta)_{\zeta=0}$ relative to the nonslender cone solution; additionally, the effect tends to increase with increasing values of the rarefaction parameter $\bar{\varkappa}$ $\left(\left[\partial\bar{u}/\partial\zeta\right]_{\zeta=0}=\alpha_0\left[1+A/2\alpha_0^2\right]\right.$ where A, the integration constant determined from the shock boundary conditions, is negative and α_0 is a power series in $\left.\bar{\varkappa}\right)$.

Also notable in Figure A-1 is the larger effect of transverse curvature for $\theta_c = 10°$, compared to $\theta_c = 20°$. The differences from the nonslender cone solution are significantly greater for both the velocity and the velocity gradient at the wall. This difference for the two cones is also evident in the heat-transfer prediction (see Figure 5 and Section 4.3).

Next, we consider the shock layer thickness, r_s/r_o, and the difference between shock angle and body angle, $\beta - \theta_c$. These have been calculated directly from the zero-order solution, Equations A-5 and A-6, and are shown in Figure A-2 as a function of the rarefaction parameter $\bar{\chi}$ for $\theta_c = 10°$ and $20°$. As the cone angle or the rarefaction parameter are decreased, the shock layer thickness relative to the body thickness and the shock angle are increased. For $\theta_c = 20°$, the value of $\frac{y_s}{r_o}$ is about 0.4, whereas for $\theta_c = 10°$, $\frac{y_s}{r_o} \simeq 1$; in the latter case particularly, this value of y_s/r_o violates considerably the assumption of a thin shock layer. The solution for shock angle and shock coordinate utilizing the perturbed velocity profiles reduces the magnitudes of these quantities, but not significantly. The first-order relation for r_1/r_o from the perturbation analysis is

$$\left(\frac{r_1}{r_o}\right)^2 = 1 + \frac{\epsilon}{\sin^2\beta}\left[\zeta^2\left(\frac{r}{r_o}\right)^2\left(1 - \bar{u}\cos^2\theta_c\right) + \cos^2\theta_c \int_0^{\zeta} \zeta^2\left(\frac{r}{r_o}\right)^2 d\bar{u}\right]$$

where r/r_o is given by the zero-order solution and the effect on r_1/r_o of $\bar{p}$ not equal to unity is neglected.

This perturbation analysis has shown that the dominant effect is that of transverse curvature and that for $\theta_c = 10°$, the assumption of a thin shock layer is violated considerably for values of the rarefaction parameter below 3.

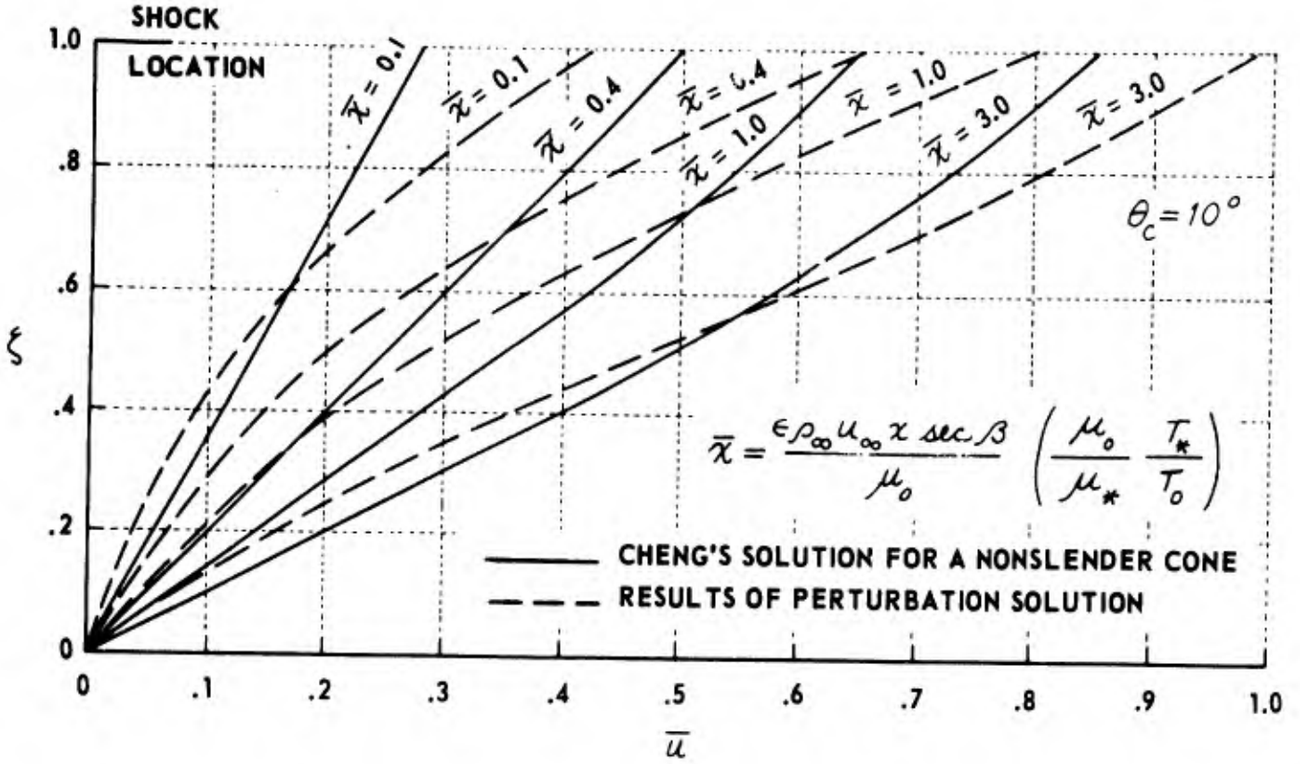

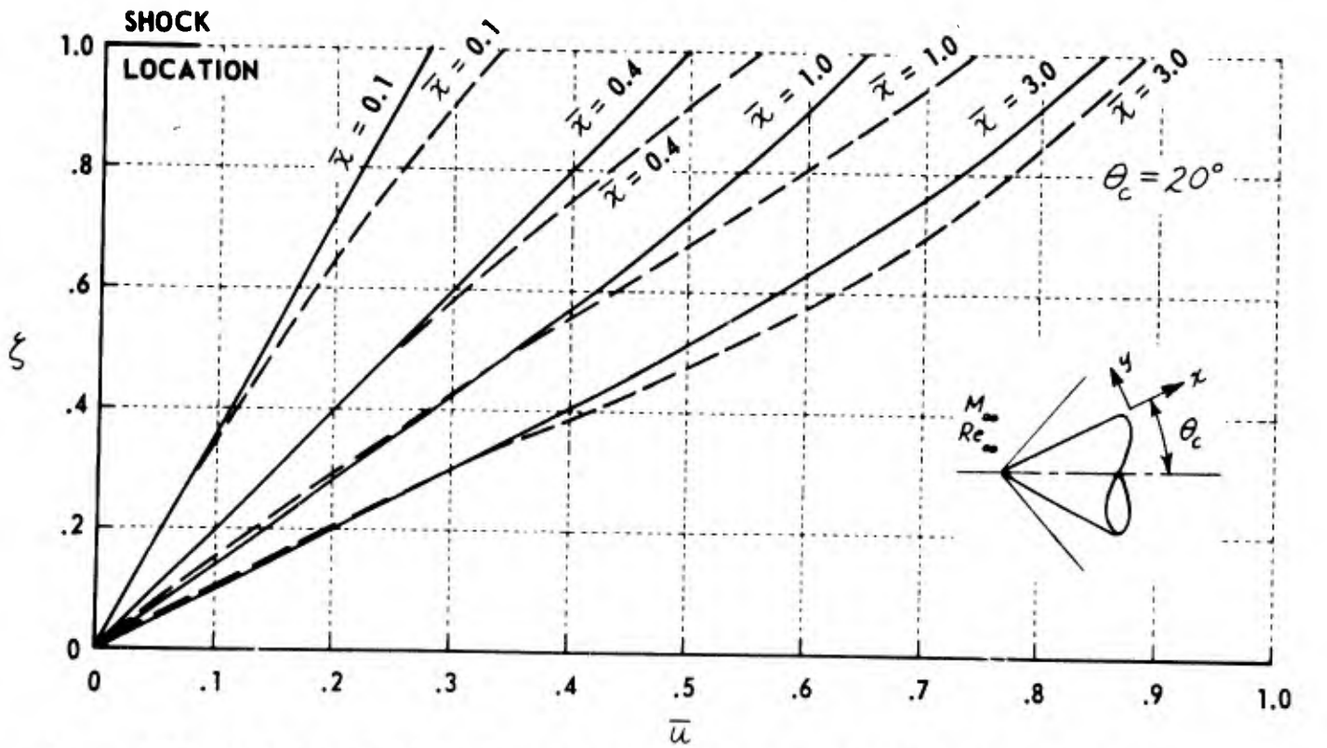

Figure A-1 VELOCITY PROFILE OVER POINTED 10° AND 20° HALF-ANGLE CONE

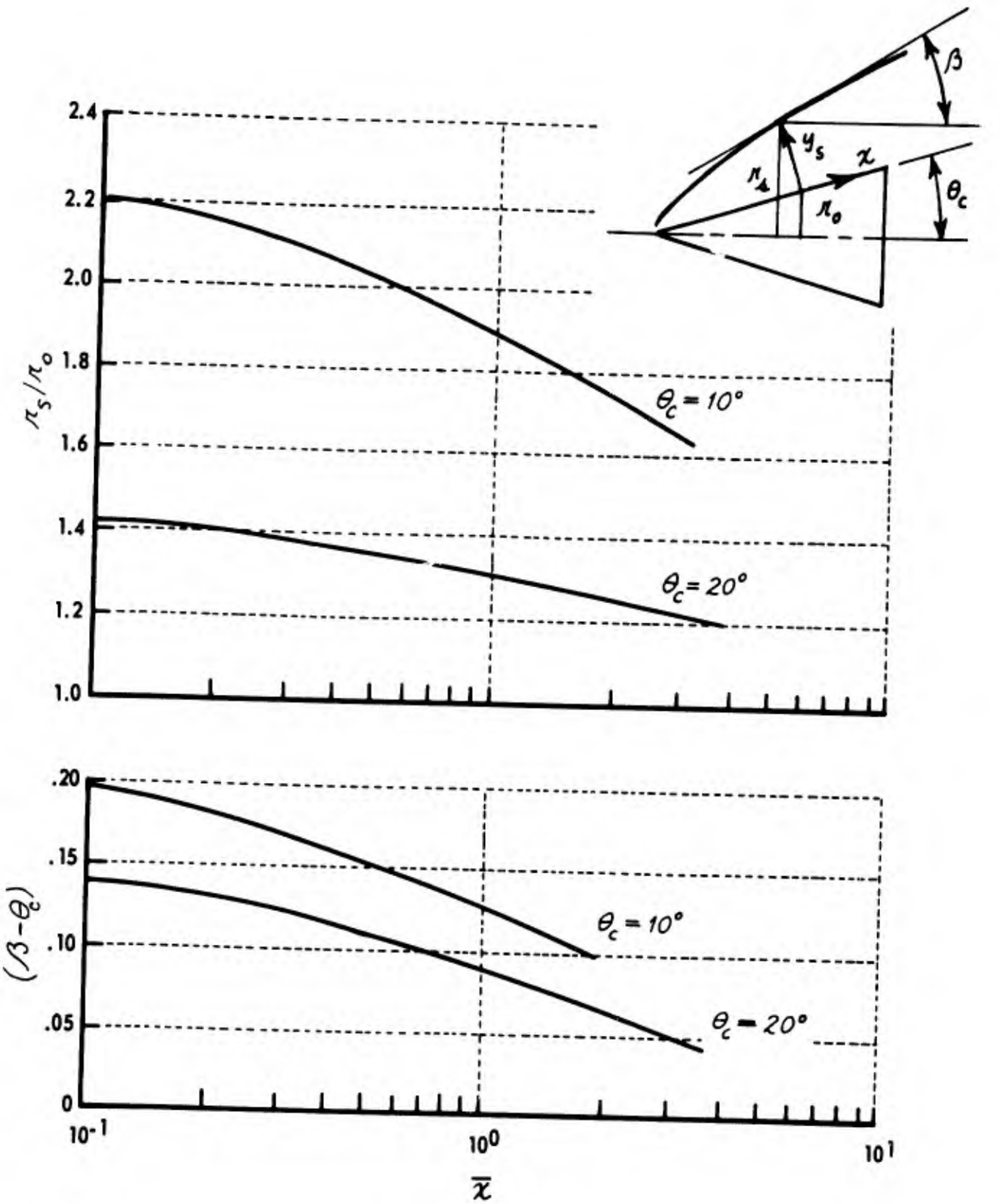

Figure A-2 PREDICTION OF SHOCK ANGLE $(\beta - \theta_c)$ AND SHOCK COORDINATE (r_s/r_o) FOR $\theta_c = 10°$ AND $\theta_c = 20°$

BLANK PAGE

Unclassified

Security Classification

DOCUMENT CONTROL DATA - R&D

(Security classification of title, body of abstract and indexing annotation must be entered when the overall report is classified)

ORIGINATING ACTIVITY (Corporate author) Cornell Aeronautical Laboratory, Inc. Buffalo, New York	2a. REPORT SECURITY CLASSIFICATION Unclassified 2b GROUP

REPORT TITLE

VISCOUS HYPERSONIC FLOWS OVER POINTED CONES AT LOW REYNOLDS NUMBERS

DESCRIPTIVE NOTES (Type of report and inclusive dates)

Scientific. Interim. January 1966

AUTHOR(S) (Last name, first name, initial)

Waldron, H. F.

6. REPORT DATE June 1966	7a. TOTAL NO. OF PAGES 39	7b. NO. OF REFS 17
8a. CONTRACT OR GRANT NO. AF 33(615)-1205 b. PROJECT NO. 7064 c. 61445014 d. 681307	9a. ORIGINATOR'S REPORT NUMBER(S) 9b. OTHER REPORT NO(S) (Any other numbers that may be assigned this report) ARL 66-0111	

10. AVAILABILITY/LIMITATION NOTICES

1. Distribution of this article is unlimited.

11. SUPPLEMENTARY NOTES	12. SPONSORING MILITARY ACTIVITY Aerospace Research Laboratories (ARR) Office of Aerospace Research United States Air Force Wright-Patterson Air Force Base, Ohio

13. ABSTRACT

An experimental and analytical study of viscous hypersonic flow over pointed cones with particular emphasis on the viscous-layer regime is presented. Shock tunnel measurements of heat transfer to 5°, 10° and 20° half-angle cones and of pressure on the 20° cone are compared with the predictions of a viscous-inviscid interaction analysis (Probstein and Elliot) including transverse curvature, of a viscous-layer nonslender cone analysis (Cheng) and of an extension of the nonslender cone analysis incorporating effects of slenderness. The large rise in heat transfer predicted by the transverse curvature theory is not observed and close agreement is obtained with the nonslender cone viscous-layer predictions. An extension of the nonslender cone analysis is presented where the effects of cone slenderness are included by a perturbation analysis. The solution of the resulting equations reveals that the net effect of transverse curvature and of other effects associated with cone slenderness is small in the viscous-layer regime for not-too-slender cones. Good agreement of the 10° and the 20° cone experimental data is obtained with this extension of the nonslender solution.

DD FORM 1 JAN 64 1473

Security Classification

14. KEY WORDS	LINK A		LINK B		LINK C	
	ROLE	WT	ROLE	WT	ROLE	WT
sharp flat plate low density flow hypersonic boundary layer flow field measurements leading edge shock wave structure ·						

INSTRUCTIONS

1. **ORIGINATING ACTIVITY:** Enter the name and address of the contractor, subcontractor, grantee, Department of Defense activity or other organization *(corporate author)* issuing the report.

2a. **REPORT SECURITY CLASSIFICATION:** Enter the overall security classification of the report. Indicate whether "Restricted Data" is included. Marking is to be in accordance with appropriate security regulations.

2b. **GROUP:** Automatic downgrading is specified in DoD Directive 5200.10 and Armed Forces Industrial Manual. Enter the group number. Also, when applicable, show that optional markings have been used for Group 3 and Group 4 as authorized.

3. **REPORT TITLE:** Enter the complete report title in all capital letters. Titles in all cases should be unclassified. If a meaningful title cannot be selected without classification, show title classification in all capitals in parenthesis immediately following the title.

4. **DESCRIPTIVE NOTES:** If appropriate, enter the type of report, e.g., interim, progress, summary, annual, or final. Give the inclusive dates when a specific reporting period is covered.

5. **AUTHOR(S):** Enter the name(s) of author(s) as shown on or in the report. Enter last name, first name, middle initial. If military, show rank and branch of service. The name of the principal author is an absolute minimum requirement.

6. **REPORT DATE:** Enter the date of the report as day, month, year; or month, year. If more than one date appears on the report, use date of publication.

7a. **TOTAL NUMBER OF PAGES:** The total page count should follow normal pagination procedures, i.e., enter the number of pages containing information.

7b. **NUMBER OF REFERENCES:** Enter the total number of references cited in the report.

8a. **CONTRACT OR GRANT NUMBER:** If appropriate, enter the applicable number of the contract or grant under which the report was written.

8b, 8c, & 8d. **PROJECT NUMBER:** Enter the appropriate military department identification, such as project number, subproject number, system numbers, task number, etc.

9a. **ORIGINATOR'S REPORT NUMBER(S):** Enter the official report number by which the document will be identified and controlled by the originating activity. This number must be unique to this report.

9b. **OTHER REPORT NUMBER(S):** If the report has been assigned any other report numbers *(either by the originator or by the sponsor)*, also enter this number(s).

10. **AVAILABILITY/LIMITATION NOTICES:** Enter any limitations on further dissemination of the report, other than those imposed by security classification, using standard statements such as:

(1) "Qualified requesters may obtain copies of this report from DDC."

(2) "Foreign announcement and dissemination of this report by DDC is not authorized."

(3) "U. S. Government agencies may obtain copies of this report directly from DDC. Other qualified DDC users shall request through

_____.

(4) "U. S. military agencies may obtain copies of this report directly from DDC. Other qualified users shall request through

_____."

(5) "All distribution of this report is controlled. Qualified DDC users shall request through

_____."

If the report has been furnished to the Office of Technical Services, Department of Commerce, for sale to the public, indicate this fact and enter the price, if known.

11. **SUPPLEMENTARY NOTES:** Use for additional explanatory notes.

12. **SPONSORING MILITARY ACTIVITY:** Enter the name of the departmental project office or laboratory sponsoring *(paying for)* the research and development. Include address.

13. **ABSTRACT:** Enter an abstract giving a brief and factual summary of the document indicative of the report, even though it may also appear elsewhere in the body of the technical report. If additional space is required, a continuation sheet shall be attached.

It is highly desirable that the abstract of classified reports be unclassified. Each paragraph of the abstract shall end with an indication of the military security classification of the information in the paragraph, represented as *(TS), (S), (C), or (U)*.

There is no limitation on the length of the abstract. However, the suggested length is from 150 to 225 words.

14. **KEY WORDS:** Key words are technically meaningful terms or short phrases that characterize a report and may be used as index entries for cataloging the report. Key words must be selected so that no security classification is required. Identifiers, such as equipment model designation, trade name, military project code name, geographic location, may be used as key words but will be followed by an indication of technical context. The assignment of links, rules, and weights is optional.

GPO 886-551